

Geometric Analysis of Population Rhythms in Synaptically Coupled Neuronal Networks

J. Rubin
D. Terman

Department of Mathematics, Ohio State University, Columbus, Ohio 43210, U.S.A.

We develop geometric dynamical systems methods to determine how various components contribute to a neuronal network's emergent population behaviors. The results clarify the multiple roles inhibition can play in producing different rhythms. Which rhythms arise depends on how inhibition interacts with intrinsic properties of the neurons; the nature of these interactions depends on the underlying architecture of the network. Our analysis demonstrates that fast inhibitory coupling may lead to synchronized rhythms if either the cells within the network or the architecture of the network is sufficiently complicated. This cannot occur in mutually coupled networks with basic cells; the geometric approach helps explain how additional network complexity allows for synchronized rhythms in the presence of fast inhibitory coupling. The networks and issues considered are motivated by recent models for thalamic oscillations. The analysis helps clarify the roles of various biophysical features, such as fast and slow inhibition, cortical inputs, and ionic conductances, in producing network behavior associated with the spindle sleep rhythm and with paroxysmal discharge rhythms. Transitions between these rhythms are also discussed.

1 Introduction ---

Neuronal networks often exhibit a rich variety of oscillatory behavior. The dynamics of even a single cell may be quite complicated; it may, for example, fire repetitive spikes or bursts of action potentials, each followed by a silent phase of near-quiet behavior (Rinzel, 1987; Wang & Rinzel, 1995). The bursting behavior may wax and wane on a slower timescale (Destexhe, Babloyantz, & Sejnowski, 1993; Bal & McCormick, 1996). Examples of population rhythms include synchronous behavior, in which every cell in the network fires at the same time, and clustering, in which the entire population of cells breaks up into subpopulations or blocks; the cells within a single block fire synchronously while different blocks are desynchronized from each other (Golomb & Rinzel, 1994; Kopell & LeMasson, 1994). Of course, much more complicated population rhythms are also possible (Traub & Miles, 1991; Terman & Lee, 1997). Activity may also propagate through the

network in a wavelike manner (Kim, Bal, & McCormick, 1995; Destexhe, Bal, McCormick, & Sejnowski, 1996; Golomb, Wang, & Rinzel, 1996; Rinzel, Terman, Wang, & Ermentrout, 1998).

A network's population rhythm results from interactions among three separate components: the intrinsic properties of individual neurons, the synaptic properties of coupling between neurons, and the architecture of coupling (i.e., which neurons communicate with each other). These components typically involve numerous parameters and multiple timescales. The synaptic coupling, for example, can be excitatory or inhibitory, and its possible turn-on and turn-off rates can vary widely. Neuronal systems may include several different types of cells, as well as different types of coupling. An important and typically challenging problem is to determine the role each component plays in shaping the emergent network behavior.

In this article we consider recent models for thalamic oscillations (see, for example, Destexhe, McCormick, & Sejnowski, 1993; Steriade, McCormick, & Sejnowski, 1993; Golomb, Wang, & Rinzel, 1994; Terman, Bose, & Kopell, 1996; Destexhe & Sejnowski, 1997). The networks consist of several types of cells and include excitatory as well as both fast and slow inhibitory coupling. One interesting property of these networks is that they exhibit very different rhythms for different parameter ranges. For some parameter values, the network behavior resembles that of the spindle sleep rhythm: one population of cells is synchronized at the spindle frequency, while another population of cells exhibits clustering. If a certain parameter, corresponding to the strength of fast inhibition, is varied, then the entire network becomes synchronized. This resembles paroxysmal discharge rhythms associated with spike-and-wave epilepsy. In other parameter ranges, the network behavior is similar to that associated with the delta sleep rhythm; in this case, each cell exhibits an entirely different behavior from before.

We develop geometric dynamical systems methods to analyze the mechanisms responsible for each of these rhythms and the transitions between them. This approach helps determine each component's contribution to the network behavior and to clarify how the behavior changes with respect to parameters. We are particularly interested in analyzing the role of inhibitory coupling in generating different oscillatory behaviors. This is done by considering a series of networks with increasing levels of complexity. Our analysis demonstrates, for example, how networks with distinct architectures can make different uses of inhibition to produce different rhythms. The techniques we develop are quite general and do not depend on the details of the specific systems. For a given network, however, these techniques lead to rather precise conditions for when a particular rhythm is possible.

Numerous work has considered the role of inhibition in synchronizing oscillations (for example, Wang & Rinzel, 1992, 1993; Golomb & Rinzel, 1993; van Vreeswijk, Abbott, & Ermentrout, 1994; Whittington, Traub, & Jefferys, 1995; Bush & Sejnowski, 1996; Gerstner, van Hemmen, & Cowan, 1996; Rowat & Selverston, 1997; Terman, Kopell, & Bose, 1998). Many of

these articles used model neurons with very short spiking times. These include integrate-and-fire models along with alpha function–type dynamics for the synapses. More biophysically based models for bursting neurons were considered by, among others, Wang and Rinzel (1993) and Terman et al. (1998). One conclusion of those works is that inhibition can lead to synchrony only if the inhibition decays at a sufficiently slow rate; in particular, the rate of decay of the synapses must be slower than the rate at which the neurons recover in their refractory period. These theoretical and numerical studies, however, considered rather idealized networks: Each cell contained only one channel state variable, and the network architecture was simply two mutually coupled cells. By considering more realistic biophysical models, we demonstrate that fast inhibitory coupling can indeed lead to synchronous rhythms. We show that this is possible in networks with complicated cells but simple architectures and in networks with more complicated architectures but simple cells.

Geometric singular perturbation methods have been used previously to study the population rhythms of neuronal networks (for example, Somers & Kopell, 1993; Skinner, Kopell, & Marder, 1994; Terman & Wang, 1995; Terman & Lee, 1997; Terman et al., 1998; LoFaro & Kopell, in press). Each of the relevant networks possess multiple timescales; this allows one to dissect the full system into fast and slow subsystems. Often, however, there is no clear-cut separation of timescales, so it is not obvious how one decides which variables should be considered as fast or slow. This is particularly the case when there are multiple intrinsic channel state variables and the synaptic variables turn on and turn off at different rates. A primary goal of this article is to demonstrate how one can make the singular reduction in order to understand mechanisms responsible for the thalamic rhythms.

Two crucial issues are related to the geometric analysis. The first is concerned with the existence of a singular solution corresponding to a particular pattern. We assume that individual cells, without any coupling, are unable to oscillate. The existence of network oscillatory behavior then depends on whether the singular trajectory is able to “escape” from the silent phase. An important point will be that greater cellular or network complexity enhances each cell’s opportunity to escape the silent phase when coupled. The second issue is concerned with the stability of the solution. To demonstrate stability of a perfectly synchronous state, for example, we must show that the trajectories corresponding to different cells are brought closer together as they evolve in phase space. As we shall see, this compression is usually not controlled by a single factor; it depends on the underlying architecture as well as nontrivial interactions between the intrinsic and synaptic properties of the cells (see also Terman et al., 1998). Our analysis demonstrates, for example, why thalamic networks are well suited to use inhibitory coupling to help synchronize oscillations and produce other, clustered, rhythms.

In the next section we describe in detail the types of models to be considered for individual neurons. We distinguish between basic and compound

cells. As a concrete example, we consider recent conductance-based models for thalamocortical relay (TC) cells (Golomb et al., 1994; Destexhe & Sejnowski, 1997 and references therein). Compound cells can be realized as a model for a TC cell that includes three ionic currents: a low-threshold calcium current (I_T), the nonselective sag current (I_{sag}), and a leak. A basic cell does not include I_{sag} . In this context, our results help to explain the role of I_{sag} in generating network activity; we shall see that this role depends on the architecture of the network. We also discuss different forms of synaptic coupling and different architectures.

In section 3, we show that synchronization is possible in mutually coupled networks that include compound cells and fast synapses. This analysis is similar to that done by Terman et al. (1998), which showed that synchronization is possible in networks with basic cells and slow inhibitory coupling. Those networks contain two types of slow processes: one corresponds to an intrinsic ionic current and the other to a synaptic slow variable. The main conclusion of the analysis here is that what is crucial for synchronization is that the network possess at least two slow processes; one may be intrinsic and the other synaptic, or both may be intrinsic.

In section 4, we consider networks with architectures motivated by recent models for the thalamic spindle sleep rhythm. The more complex architectures allow the network to use inhibition in different ways to produce different population rhythms. In particular, inhibition can play an important role in synchronizing the cells in a much more robust way than in the mutually coupled networks. We demonstrate how tuning various parameters allows the network to control the effect of inhibition and thereby control the emergent behavior.

Consequences of these results for the full thalamic networks are presented in section 5. We consider the roles of various biophysical parameters associated with fast and slow inhibition, the sag current, cortical inputs, and other currents. These results help clarify the mechanisms responsible for spindle and paroxysmal discharge rhythms and the ways that changes in biophysical parameters lead to transitions between different rhythms. We conclude with a discussion in section 6.

2 The Models

We begin by describing the equations corresponding to individual cells and then describe the synaptic coupling between two cells. It is necessary to explain which parameters determine whether the synapse is excitatory or inhibitory and which other parameters determine whether the synapse is fast or slow. It will also be necessary to distinguish between direct synapses and indirect synapses. Finally, we describe the types of architectures to be considered.

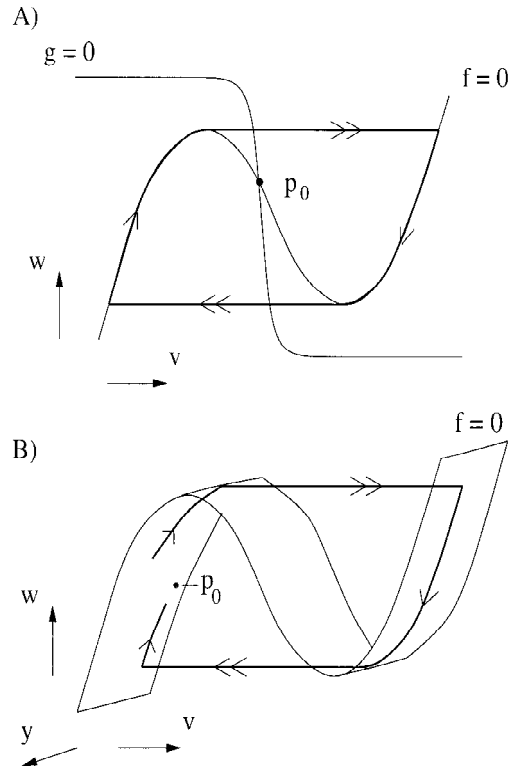


Figure 1: Nullclines of basic and compound cells. (A) The v - and w -nullclines of a basic cell intersect at p_0 , on the middle branch of the v -nullcline, in the oscillatory case. The closed curve indicates a singular periodic orbit, with double arrows denoting fast pieces and single arrows denoting slow pieces. (B) The v -nullcline and a singular solution of an excitable compound cell with a stable critical point p_0 .

2.1 Single Cells. We model a basic cell as the relaxation oscillator

$$\begin{aligned} v' &= f(v, w) \\ w' &= \epsilon g(v, w), \end{aligned} \quad (2.1)$$

where $' = \frac{d}{dt}$. Here ϵ is assumed to be small; hence, w represents a slowly evolving quantity. The active phase of the oscillation can be viewed as the envelope of a burst of spikes. We assume that the v -nullcline, $f(v, w) = 0$, defines a cubic-shaped curve, as shown in Figure 1A, and the w -nullcline, $g = 0$, is a monotone decreasing curve that intersects $f = 0$ at a unique point p_0 . We also assume that $f > 0$ ($f < 0$) above (below) the v -nullcline and

$g > 0$ (< 0) below (above) the w -nullcline. If p_0 lies on the middle branch of $f = 0$, then equation 2.1 gives rise to a periodic solution for all ϵ sufficiently small, and we say that the system is oscillatory. In the limit $\epsilon \rightarrow 0$, one can construct a singular solution as shown in Figure 1A. If p_0 lies on the left branch of $f = 0$, then the system is said to be excitable; p_0 is a stable fixed point, and there are no periodic solutions for all ϵ small. Note that the thalamic cells we seek to model are typically excitable during the sleep state. For some of our results, it will be necessary to make some more technical assumptions on the nonlinearities f and g . We will sometimes assume that

$$f_w > 0, \quad g_v < 0 \quad \text{and} \quad g_w < 0 \quad (2.2)$$

near the singular solutions.

By a compound cell we mean one that contains at least two slow processes. We consider compound cells that satisfy equations of the form

$$\begin{aligned} v' &= f(v, w, y) \\ w' &= \epsilon g(v, w) \\ y' &= \epsilon h(v, y). \end{aligned} \quad (2.3)$$

Precise assumptions required on the nonlinear functions in equation 2.3 are given later. For now, we assume that for each fixed value of y , the functions $f(v, w, y)$ and $g(v, w)$ satisfy the conditions described for a basic cell. Then $\{f(v, w, y) = 0\}$ defines a cubic-shaped surface. The system (see equation 2.3) is said to be excitable if there exists a unique fixed point, which we denote by p_0 , and this lies on the left branch of the cubic-shaped surface. One can construct singular solutions of this equation, and one of these is shown in Figure 1B. The singular solution shown begins in the silent phase, or left branch, of the surface. It evolves there until it reaches the curve of jump-up points that correspond to the left knees of the cubic surface. The singular solution then jumps up to the active phase, or right branch, of the surface. It evolves in the active phase until it reaches the jump-down points or right knees of the surface. It then evolves in the silent phase, approaching the stable fixed point at p_0 . A more formal description of certain singular solutions is given in section 3.2.

2.2 Synaptic Coupling. Consider the network of two mutually coupled cells: $E_1 \leftrightarrow E_2$. The equations corresponding to this network are

$$\begin{aligned} v_1' &= f(v_1, q_1) - g_{syn} s_2 (v_1 - v_{syn}) \\ q_1' &= \epsilon \Lambda(v_1, q_1) \\ v_2' &= f(v_2, q_2) - g_{syn} s_1 (v_2 - v_{syn}) \\ q_2' &= \epsilon \Lambda(v_2, q_2). \end{aligned} \quad (2.4)$$

Here, $q_i = w_i$ and $\Lambda = g$ if the cells are basic, while $q_i = (w_i, y_i)$ and $\Lambda = (g, h)$ if the cells are compound. In equation 2.4, $g_{syn} > 0$. It is the parameter v_{syn} that determines whether the synapse is excitatory or inhibitory. If $v_{syn} < v$ along each bounded singular solution, then the synapse is inhibitory.

The coupling depends on the synaptic variables s_i , $i = 1, 2$. We consider two choices for the s_i . Each s_i may satisfy a first-order equation of the form

$$s_i' = \alpha(1 - s_i)H(v_i - \theta_{syn}) - \beta s_i. \quad (2.5)$$

Here, α and β are positive constants, H is the Heaviside step function, and θ_{syn} is a threshold above which one cell can influence the other. Note that α and β are related to the rates at which the synapses turn on or turn off. For fast synapses, we assume that α is $O(1)$ with respect to ϵ . It may seem natural also to assume that β is $O(1)$, and this is, in fact, what we will do in the next section. However, when we consider the thalamic networks in sections 4 and 5, it will be necessary to assume that $\beta = K\epsilon$, where K is a large constant. The reason for choosing the fast synaptic variables in this way is discussed in more detail later. (The model for slow synapses is discussed in section 5.2.)

If the synaptic variables satisfy equation 2.5, then we say that the synapse is direct. We will also consider indirect synapses. These are modeled by introducing a second synaptic variable x_i (see Golomb et al., 1994; Terman et al., 1998). The equations for (x_i, s_i) are:

$$\begin{aligned} x_i' &= \epsilon\alpha_x(1 - x_i)H(v_i - \theta_{syn}) - \epsilon\beta_x x_i \\ s_i' &= \alpha(1 - s_i)H(x_i - \theta_x) - \beta s_i. \end{aligned} \quad (2.6)$$

Here, α_x and β_x are positive constants. Note that indirect synapses have the effect of introducing a delay in the synaptic action, and this delay takes place on the slow timescale. If, say, the cell E_1 fires, then x_1 will activate once v_1 crosses the threshold θ_{syn} . The activation of s_1 must wait until x_1 crosses the second threshold θ_x . Note also that an indirect synapse can be fast if α and β are $O(1)$, as discussed above.

2.3 Globally Inhibitory Networks. Besides mutually coupled networks, we also consider networks with the architecture shown in Figure 2. This network contains two different types of cells, labeled E -cells and J -cells. Each E -cell sends fast excitation to some of the J -cells, and each J -cell sends inhibition to some of the E -cells. The inhibition may be fast or slow (or both). There is no communication among different E -cells; however, the J -cells communicate with each other via fast inhibitory coupling.

This network is motivated by recent models for the thalamic sleep rhythms discussed in section 1. The E - and J -cells correspond to thalamocortical relay (TC) and thalamic reticularis (RE) cells, respectively.

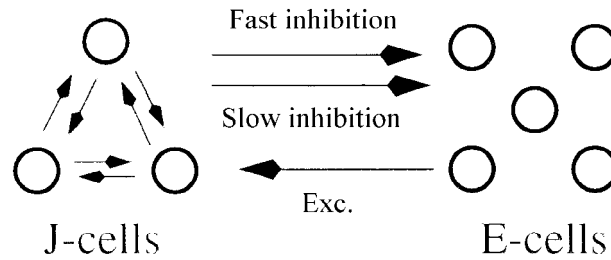


Figure 2: Network of inhibitory *J*-cells and excitatory *E*-cells.

3 Mutually Coupled Compound Cells with Fast Inhibitory Synapses —

Rubin and Terman (1998) proved that stable synchronous oscillations are not possible in mutually coupled networks with fast inhibitory coupling and only one slow variable corresponding to each cell. This holds regardless of whether the cells are excitable or oscillatory and whether the synapses are direct or indirect. These results are for networks with relaxation-type neurons, as discussed in the previous section.

Here we demonstrate that when the mutually coupled cells are compound, they can exhibit synchronized oscillations when connected with fast inhibitory coupling. The synchronous solution may exist if the synapses are direct, but as in Terman et al. (1998), it can be stable only if the synapses are indirect (see section 3.3). We assume that each cell is excitable for fixed levels of input; however, there is no problem in extending the analysis if this does not hold. We analyze the network by constructing singular solutions, done by piecing together solutions of reduced fast and slow subsystems. Since the cells are compound, there will be at least two slow variables corresponding to each cell. The multiple slow variables are needed for both the existence and the stability of the synchronous solution. For existence, the multiple slow variables allow the singular trajectory to escape from the silent phase, despite the fact that each cell is excitable. The multiple slow variables also allow for several mechanisms that lead to compression of cells as they evolve in phase-space.

We do not give precise conditions on the parameters and nonlinearities in the equations to specify when the synchronous solution is stable, as was done in Terman et al. (1998). This will be done elsewhere. Here we describe the geometric mechanisms that allow the cells to escape the silent phase so a synchronous solution is possible and then characterize the compression mechanisms that act to stabilize the synchronous solution. A primary aim of this article is to compare how inhibition is used in different networks with different architectures to produce stable synchrony. By identifying the compression mechanisms here, we are able to evaluate the robustness of the

synchronous solution. As we shall see, the compression mechanisms for the mutually coupled architecture are considerably less robust than those that arise in the globally inhibitory thalamic networks.

The analysis here is similar to but more general than that in Terman et al. (1998), where it is demonstrated that stable synchrony can arise in networks with basic cells but slow synapses. It is assumed in Terman et al. (1998) that the synapses activate on the fast timescale and that the evolution of the cells in the active phase does not depend on the level of synaptic input. These assumptions imply that the slow system corresponding to the active phase is one-dimensional. We do not make these assumptions here and demonstrate that the resulting richer dynamics may lead to additional compression mechanisms for stabilizing the synchronous solution.

3.1 Singular Solutions. We analyze the network by treating ϵ as a small, singular perturbation parameter and constructing singular solutions. These consist of various pieces, each piece corresponding to a solution of either fast or slow equations. The fast equations are obtained by simply letting $\epsilon = 0$ in equation 2.4 and in either equation 2.5 or 2.6. The slow equations are obtained by replacing t with $\tau = \epsilon t$ as the independent variable and then letting $\epsilon = 0$. We assume here that both α and β are independent of ϵ . There is no problem in extending this analysis if $\beta = O(\epsilon)$; this is actually an easier case since the additional slow variable then provides additional opportunities for compression. Here we derive the reduced slow equations valid when the synapses are direct. The equations for indirect synapses are similar, but there are more cases to consider.

The slow equations are

$$\begin{aligned} 0 &= f(v_i, w_i, y_i) - g_{syn}s_j(v_i - v_{syn}) \\ \dot{w}_i &= g(v_i, w_i) \\ \dot{y}_i &= h(v_i, y_i) \\ 0 &= \alpha(1 - s_i)H(v_i - \theta_{syn}) - \beta s_i, \end{aligned} \quad (3.1)$$

where $\dot{} = \frac{d}{d\tau}$. One can reduce this system to equations for just the slow variables (y_i, w_i) . There are several cases to consider depending on whether both cells are silent, both are active, or one is silent and the other is active. We assume that the solution of the first equation in 3.1 defines a cubic-shaped surface \mathcal{C}_s , and the left and right branches of this surface can be expressed as $v_i = \Phi_L(w_i, y_i, s_i)$ and $v_i = \Phi_R(w_i, y_i, s_i)$, respectively.

If both cells are silent, then each $v_i < \theta_{syn}$ and $s_i = 0$. Let $G_L(w, y, s) \equiv g(\Phi_L(w, y, s), w)$ and $H_L(w, y, s) \equiv h(\Phi_L(w, y, s), y)$. Then each (w_i, y_i) satisfies the equations

$$\dot{w} = G_L(w, y, 0) \quad \dot{y} = H_L(w, y, 0). \quad (3.2)$$

If both cells are active, then each $v_i > \theta_{syn}$ and the last equation in 3.1 implies that $s_i = \sigma_A \equiv \alpha/(\alpha + \beta)$. Let $G_R(w, y, s) \equiv g(\Phi_R(w, y, s), w)$ and $H_R(w, y, s) \equiv h(\Phi_R(w, y, s), y)$. Then each (w_i, y_i) satisfies the equations

$$\dot{w} = G_R(w, y, \sigma_A) \quad \dot{y} = H_R(w, y, \sigma_A). \quad (3.3)$$

Finally suppose that one cell, say cell 1, is silent and cell 2 is active. Then the slow variables satisfy the reduced equations

$$\begin{aligned} \dot{w}_1 &= G_L(w_1, y_1, \sigma_A) & \dot{w}_2 &= G_R(w_2, y_2, 0) \\ \dot{y}_1 &= H_L(w_1, y_1, \sigma_A) & \dot{y}_2 &= H_R(w_2, y_2, 0). \end{aligned} \quad (3.4)$$

We may view the singular solution as two points moving around in the (y, w) slow phase-space. Each point corresponds to the projection of one of the cells onto the slow phase plane. The points evolve according to one of the reduced slow systems until one of the points reaches a jump-up or jump-down curve. The cells then jump in the full phase-space; however, the slow variables remain constant during the fast transitions. The points then “change directions” in slow phase-space and evolve according to some other reduced slow equations.

Since the cells are excitable, the reduced system, equation 3.2, with $s = 0$ has a stable fixed point, which we denote by P_0 . The slow phase-space corresponding to equation 3.2 is illustrated in Figure 3A. Note that while some of the trajectories are attracted toward P_0 , others are able to reach the jump-up curve. That is, although the uncoupled cells are excitable, it is possible for a cell to begin in the silent phase and still fire. This will be important in the next section, when we discuss the existence of the synchronous solution.

The following lemma characterizes the left and right folds (or jump-up and jump-down curves) of C_s . We assume here that $f_y > 0$ on the left branch of C_s while $f_y < 0$ on the right. This assumption is justified, based on biophysical considerations, in remark 4 (in appendix A).

Lemma. *The left and right folds of C_s can be expressed as $J_L = \{(v_L(y, s), w_L(y, s), y)\}$ and $J_R = \{(v_R(y, s), w_R(y, s), y)\}$ where $\frac{\partial w_L}{\partial y} < 0$, $\frac{\partial w_L}{\partial s} > 0$, $\frac{\partial w_R}{\partial y} > 0$, and $\frac{\partial w_R}{\partial s} > 0$.*

Proof. Since $v_L(y, s) = \Phi_L(w_L(y, s), y, s)$, it follows from equation 3.1 and the definition of folds that

$$\begin{aligned} 0 &= f(\Phi_L(w_L(y, s), y, s), w_L(y, s), y) - g_{syn} s (\Phi_L(w_L(y, s), y, s) - v_{syn}) \\ 0 &= f_v(\Phi_L(w_L(y, s), y, s), w_L(y, s), y) - g_{syn} s \end{aligned} \quad (3.5)$$

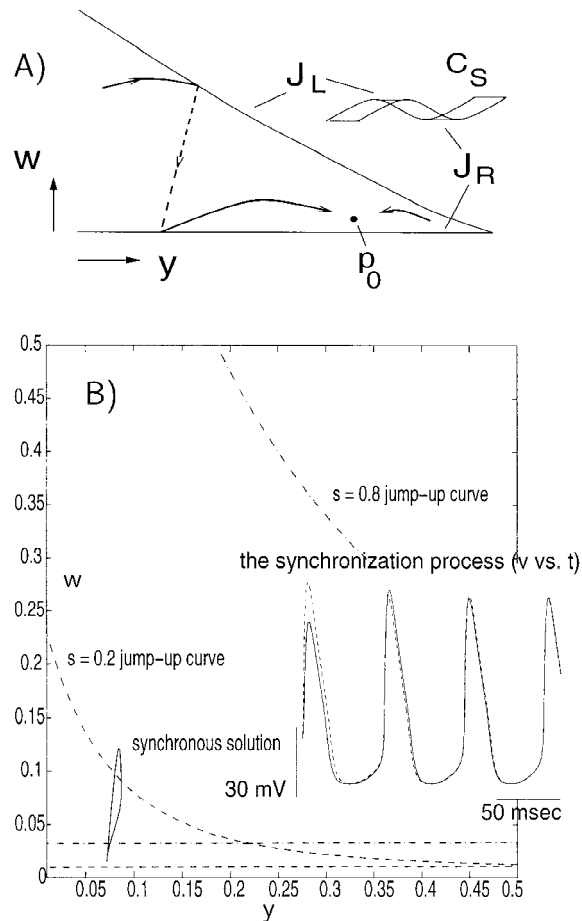


Figure 3: Singular solutions for compound cells. (A) The slow phase-space of an uncoupled compound cell, bounded by the jump-up curve J_L and the jump-down curve J_R of the slow manifold C_S . The solid (dashed) curves represent evolution in the silent (active) phase. P_0 is a stable fixed point. (B) Numerically generated synchronous solution for mutually coupled compound cells that are separately excitable, in (y, w) -space. The inset (v versus t) shows the voltage traces as two cells approach synchrony. These curves, as well as those in other figures, were generated using the program XPPAUT, developed by G. B. Ermentrout, with parameter values given in appendix A. The solid curve is the synchronous solution, the dashed curves are the jump-up (labeled) and jump-down (approximately horizontal, unlabeled) curves for $s = 0.2$, and the dash-dotted curves (partially obscured) are those for $s = \sigma_A = 0.8$. Note that the curves for $s = 0.8$ lie at larger w -values than those for $s = 0.2$. Since $\epsilon \neq 0$, the synchronous solution does not jump up [$y' = 0$, near $(y, w) = (0.08, 0.07)$] immediately on reaching the jump-up curve.

Differentiating the first equation in 3.5 with respect to w and using the second equation, we obtain

$$0 = \frac{\partial f}{\partial w} \frac{\partial w_L}{\partial s} - g_{syn}(\Phi_L(w_L(y, s), y, s) - v_{syn}).$$

Hence,

$$\frac{\partial w_L}{\partial s} = \frac{g_{syn}(\Phi_L(w_L(y, s), y, s) - v_{syn})}{f_w}. \quad (3.6)$$

The right-hand side of this expression has a positive numerator because the coupling is inhibitory and a positive denominator from equation 2.2, so $\frac{\partial w_L}{\partial s} > 0$. Analogously, $\frac{\partial w_R}{\partial s} > 0$.

Similarly, differentiating with respect to y in equation 3.5 yields $0 = \frac{\partial f}{\partial w} \frac{\partial w_L}{\partial y} + \frac{\partial f}{\partial y}$, or $\frac{\partial w_L}{\partial y} = -\frac{f_y}{f_w}$, with f_y and f_w evaluated on J_L . Analogously, $\frac{\partial w_R}{\partial y} = -\frac{f_y}{f_w}$, with f_y, f_w evaluated on J_R . The above assumptions on f_y , together with equation 2.2, yield the desired result.

Remark 1. In the thalamic networks of interest, the jump-down curve J_R is nearly horizontal (see Figure 3B). This holds because the y current has a much smaller reversal potential and maximal conductance than the w current; when a cell is in the active phase, this implies that $|f_y| \ll |f_w|$, so $|\frac{\partial w_R}{\partial y}|$ is quite small. (See remark 5 in appendix A.)

3.2 Existence of the Synchronous Solution. Here we illustrate why it is possible for a synchronous solution to exist in a network of mutually coupled compound cells even when the individual cells are excitable. A numerically generated picture of such a solution, projected onto the slow variables (y, w) , is shown together with certain jump-up and jump-down curves in Figure 3B. We also show a solution with initial conditions slightly perturbed from the synchronous solution. The precise equations that this solution satisfies and the parameter values used numerically are given in appendix A.

One constructs the singular synchronous solution as follows. We begin when the cells are in the silent phase, just after they have jumped down. The slow variables then evolve according to equation 3.2. If they are able to reach the jump-up curve, then they jump up according to the fast equations. While in the active phase, the slow variables satisfy equation 3.3 until they reach the jump-down curve. They then jump down according to the fast equations, and this completes one cycle of the synchronous solution. Note that w and y are decreasing in the active phase and then increase just after jump-down; we use this in the next subsection.

It is not clear how to choose the starting point $(y_i(0), w_i(0))$ so that the singular orbit returns precisely to this point after one cycle. Note, however, that the variables y_i relax very close to $y_i = 0$ during the active phase. If we suppose that $y_i \approx 0$ at the jump-down point, then the value of w_i is determined; that is, for the coupled cells, $w_i \approx w_R(0, \sigma_A)$. A straightforward fixed-point argument shows that the synchronous solution will therefore exist if the solutions of equation 3.2, which begin near $(y_i, w_i) = (0, w_R(0, \sigma_A))$, are able to reach the curve of jump-up points.

The reason that a synchronous solution can exist even when the uncoupled cells cannot oscillate is that the synchronous solution lies on a different cubic during the active phase than the uncoupled cells. For this reason, the synchronous solution jumps down along a different curve than the uncoupled cells do. From the lemma, the jump-down curve $J_R(\sigma_A)$ has larger values of w than the jump-down curve $J_R(0)$ (see Figure 3B). It is therefore possible for the coupled cells to jump down to a point from which they are able eventually to escape the silent phase, although the uncoupled cells jump down to a point from which they cannot escape.

There is a nice biophysical interpretation for why coupled excitable cells may be able to oscillate. Recall that a thalamocortical relay cell is an example of a compound cell. (See section 5 for a more detailed discussion.) Then w corresponds to the inactivation variable of the I_T current. A larger value of w means that this current is more deinactivated. This implies that if the cells jump down at a larger value of w , then it is easier for the cells to become sufficiently depolarized so they can reach threshold and fire.

The construction of the synchronous solution for indirect synapses is very similar. The only difference is that after the cells jump up or jump down, there is a delay until the inhibition either turns on or turns off. The cells switch their cubic surface while in the silent and active phases, assuming that the delay is shorter than the time that the cells spend in each of their silent and active phases. We will assume that this is the case throughout the remainder of this article.

3.3 Stability of the Synchronous Solutions. We assume throughout this section that the synapses are indirect. The synchronous solution cannot be stable if the synapses are direct for the following reason. Suppose we start with both oscillators in the silent phase and assume that cell 1 jumps up. If the synapse is direct, then s_2 jumps instantly (with respect to the slow timescale) to $s_2 = 1$. The effect of this is to move cell 2 instantly away from its firing threshold, thus destabilizing the synchronous solution. Indirect synapses are needed for stability since they provide a window of opportunity for both cells to jump up during the same cycle. However, this does not guarantee that the synchronous solution is stable. One must still show that cells that are initially close together are brought closer together, or compressed, as they evolve in phase-space.

It is not at all obvious how to define *compression*. We need to demonstrate that the cells are brought closer together; however, this requires that we have a notion of distance between the cells. There are several possible metrics, each with certain advantages on different pieces of the solution. One obvious metric is the Euclidean distance between the points in phase-space corresponding to the cells. It is sometimes convenient to work with a time metric; the “distance” between the cells is then the time it takes for one cell to reach the initial position of the other cell. This was used previously in Somers & Kopell (1993), Terman & Wang (1995), Terman et al. (1998), and LoFaro & Kopell (in press).

Here, we describe several mechanisms for compression, each corresponding to a different piece of the singular solution. These mechanisms illustrate how the geometry of the two-dimensional slow subsystem, notably its curves of knees, allows for compression in the presence of inhibitory coupling. By identifying the compression mechanisms, we can then understand how changing parameters in the equations influences the stability of solutions. We can also compare the robustness of the compression mechanisms for this network with that for other networks with other architectures.

3.3.1 The Jump Up. Suppose that cell 1 lies on the jump-up curve when $\tau = 0$. After cell 1 fires, there is a delay in the onset of inhibition. We assume that cell 2 begins in the silent phase so close to the jump-up curve that it fires before it feels this inhibition. Suppose that cell 2 fires when $\tau = T_0$. We now need to make an assumption on the nonlinearities. Let (y^*, w^*) be the point where the synchronous solution jumps up. We assume that

$$(A) \quad |G_L(y^*, w^*, 0)| < |G_R(y^*, w^*, 0)| \quad \text{and} \quad |H_L(y^*, w^*, 0)| < |H_R(y^*, w^*, 0)|$$

Note that this assumption implies that the w and y coordinates of both cells change at a faster rate in the active phase after the jump up than in the silent phase before the jump up. This is certainly satisfied for the example described in appendix A and is similar to assumptions in previous work (see, for example, Somers & Kopell, 1993, where the notion of fast threshold modulation is introduced).

There are now several cases to consider depending on the orientation of the cells both before and after they jump up. We work out two of these in detail. These are the cases that arise most often for the system described in appendix A. Similar analysis applies to other cases.

Assume that $w_1(0) < w_2(T_0) < w_2(0)$ and $y_2(0) < y_1(T_0) < y_1(0)$ (see Figure 4A). These assumptions, together with the lemma, imply that $|y_1(T_0) - y_2(T_0)| < |y_1(0) - y_2(0)|$ so there is compression in the y -coordinates after the jumps. From assumption A, there is also compression in a time metric corresponding to the y -coordinate. For each τ_0 , let $\rho_y(\tau_0)$ be the time it takes for cell 2 to evolve from its position at $\tau = \tau_0$ until its y -coordinate is that of cell 1 when $\tau = \tau_0$. It then follows that $\rho_y(T_0) < \rho_y(0)$.

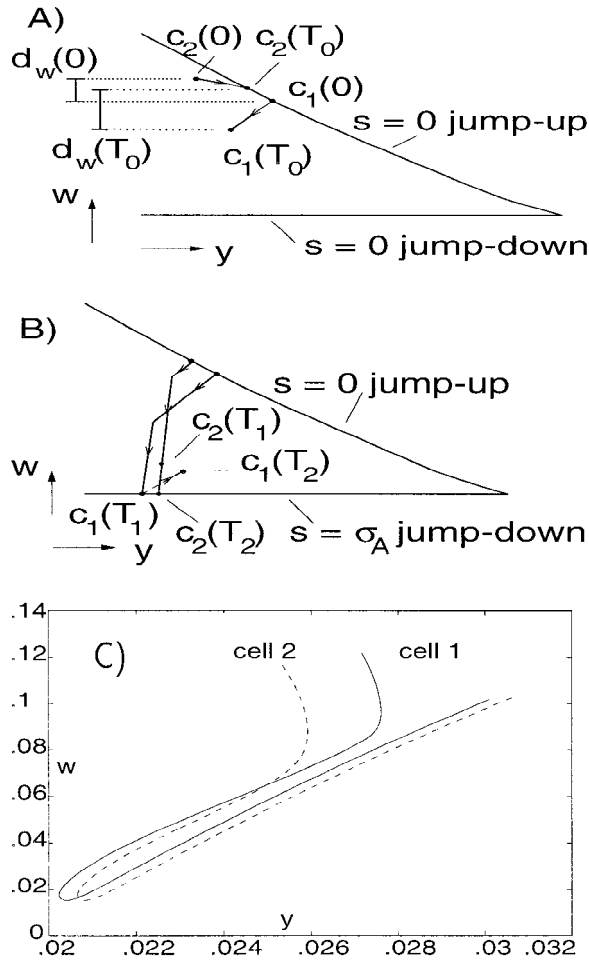


Figure 4: Compression mechanisms for mutually coupled compound cells. (A) Compression in the time metric ρ_w can occur between mutually coupled compound cells in the jump-up. Note that $w_1(0) < w_2(T_0) < w_2(0)$ and $y_2(0) < y_1(T_0) < y_1(0)$. The Euclidean distances $d_w(0)$, $d_w(T_0)$ are used to compute the time metrics $\rho_w(0)$, $\rho_w(T_0)$, respectively. (B) A reversal of orientation in the active phase (solid lines) can lead to compression in the jump-down; the dashed line indicates evolution of cell 1 in the silent phase. (C) Numerically computed trajectories of a pair of mutually coupled compound cells undergoing order reversal. Cells 1, 2 correspond to c_1 , c_2 respectively in (B). Parameter values are given in appendix A.

We now show that there is also a compression in the time metric corresponding to the w -coordinate. This is denoted by $\rho_w(\tau)$. Let $a^- = |G_L(y^*, w^*, 0)|$ and $a^+ = |G_R(y^*, w^*, 0)|$. Then

$$\begin{aligned}
\rho_w(0) &\approx \frac{w_2(0) - w_1(0)}{a^-} = \frac{w_2(0) - w_2(T_0)}{a^-} + \frac{w_2(T_0) - w_1(0)}{a^-} \\
&\approx T_0 + \frac{w_2(T_0) - w_1(0)}{a^-} > T_0 + \frac{w_2(T_0) - w_1(0)}{a^+} \\
&\approx \frac{w_1(0) - w_1(T_0)}{a^+} + \frac{w_2(T_0) - w_1(0)}{a^+} \\
&\approx \rho_w(T_0).
\end{aligned} \tag{3.7}$$

Now suppose that $w_1(0) < w_2(T_0) < w_2(0)$ and $y_1(T_0) < y_2(0)$. The exact same calculation given in equation 3.7 shows that there is compression in the time metric ρ_w across the jump up. A simple calculation also shows that there is compression in ρ_y .

3.3.2 The Active Phase. Next assume that the cells are active with $x_i > \theta_x$. Then each (y_i, w_i) satisfies equation 3.3. It is easy to see why the cells are compressed in the Euclidean metric if we make some simplifying assumptions concerning the nonlinear functions g and h . These assumptions arise naturally if one considers the network in appendix A; it is also a simple matter to extend this analysis to more general systems.

Suppose that g and h are of the form $g(v, w) = (w_\infty(v) - w)/\tau_w(v)$ and $h(v, y) = (y_\infty(v) - y)/\tau_y(v)$. Note that while in the active phase, $y_\infty(v)$ and $w_\infty(v)$ are very small. Moreover, $\tau_y(v)$ and $\tau_w(v)$ are nearly constant. We assume here that while in the active phase, $g(v, w) = -w/\tau_w$ and $h(v, y) = -y/\tau_y$, where τ_w and τ_y are positive constants. It follows that each (w_i, y_i) satisfies simple linear equations. If we ignore the jump-down curve, then each slow variable decays to 0 at an exponential rate. In particular, the distance between the cells decays exponentially. Actually, more is true. Each (y_i, w_i) approaches the origin tangent to the weakest eigendirection.

Now suppose that the jump-down curve passes close to the origin. The Euclidean distance between the cells still decreases exponentially, and both cells jump down at nearly the same point. This is the point where the jump-down curve crosses the weakest eigendirection.

We note that there is also a more subtle source of compression while the cells are active. There will be some period of time when cell 2 receives inhibition but cell 1 does not; that is, $s_1 = \sigma_A$ but $s_2 = 0$. During this time, the (y_i, w_i) satisfy different equations. It is then possible that the trajectories $(y_i(\tau), w_i(\tau))$ cross in the slow phase-space. This leads to a reversal of orientation between the cells, as shown in Figure 4B. Next, we discuss why a reversal of orientation can lead to compression in the cells' trajectories.

3.3.3 The Jump Down. We now show that if the cells reverse their orientation while in the active phase, this can lead to a form of compression after the cells jump down. Let T_i be the time when cell i jumps down. As above, assume that cell 1 jumped up first with $w_1(0) < w_2(0)$. We will assume that $w_1(\tau) < w_2(\tau)$ as long both cells are active. Moreover, from remark 1, the jump-down curve is nearly horizontal. Hence, cell 1 jumps down first; that is, $T_1 < T_2$.

If the cells' trajectories cross while in the active phase, then $y_1(T_1) < y_2(T_2)$. This is shown in Figure 4B. Let $\rho_y^A(T_1)$ be the time it would take for the solution of equation 3.3 starting at $(y_2(T_1), w_2(T_1))$ to reach the y -coordinate $y_1(T_1)$. It follows that $\rho_y^A(T_1) > T_2 - T_1$.

For $T_1 < \tau < T_2$, cell 1 evolves in the silent phase with y increasing, while cell 2 evolves in the active phase with y decreasing. If $y_1(T_2) < y_2(T_2)$, then $|y_2(T_2) - y_1(T_2)| < |y_2(T_1) - y_1(T_1)|$ so there is compression in the y -coordinates of the cells across the jump. Now suppose that $y_1(T_2) > y_2(T_2)$, as shown in Figure 4B. Let $\rho_y^S(T_2)$ be the time it would take for the solution of equation 3.2 starting at $(y_2(T_2), w_2(T_2))$ to reach the y -coordinate of cell 1. Since $y_2(T_1) > y_1(T_1)$, it follows that $\rho_y^S(T_2) < T_2 - T_1$. We have now demonstrated that $\rho_y^S(T_2) < T_2 - T_1 < \rho_y^A(T_1)$. That is, there is compression in the time metric corresponding to the y -coordinate. We note that since the jump-down curve is nearly horizontal, any compression in the w -coordinates is, to first order, neutral.

A numerical example of orientation reversal in two cells' trajectories in (y, w) -space is shown in Figure 4C. At the top of the figure, the cells are in the silent phase. Each cell jumps up where the corresponding $y'_i = 0$; chronologically, cell 1 jumps up first. In the active phase, the trajectories cross, because the cells experience different levels of inhibition; cell 2 receives inhibition first. The paths cross again at the bottom left of the figure after the leading cell, cell 1, falls down to the silent phase.

3.3.4 The Silent Phase. Suppose that both cells lie in the silent phase with $x_i < \theta_{syn}$. Then each (y_i, w_i) satisfies equation 3.2 until one of them reaches the jump-up curve. We now define a metric between the cells and, in appendix B, we analyze how to choose parameters to guarantee that the metric decreases as the cells evolve in the silent phase. This metric is similar to that introduced by Terman et al. (1998).

Suppose that cell 1 reaches the jump-up curve first, and this is at the point (y_1^*, w_1^*) . (See Figure 13 in appendix B.) Fix some time τ_0 , and let $w_L^{\tau_0}$ be the physical translate of the jump-up curve such that (y_1^*, w_1^*) is translated to the point $(y_1(\tau_0), w_1(\tau_0))$. Then the "distance" between $(y_1(\tau_0), w_1(\tau_0))$ and $(y_2(\tau_0), w_2(\tau_0))$ is the time it takes for the solution of equation 3.2, which begins at $(y_2(\tau_0), w_2(\tau_0))$, to cross $w_L^{\tau_0}$. This is certainly well defined as long as the two cells are sufficiently close to each other.

One can compute explicitly how this metric changes as the cells evolve in the silent phase. (The computation, rather technical, is in appendix B.) A more complete discussion of how this metric is used to prove the stability of the synchronous solution of two mutually coupled basic cells with slow synapses is given in Terman et al. (1998).

3.4 Further Remarks. The compression of cells can take place as the cells evolve along the multidimensional slow manifold or as they jump up or down. The compression during the jumping process depends on the geometry (or slope) of the curve of knees and the orientation of the cells both before and after the jumps. Parameters that determine this slope may therefore have subtle effects on the stability of the synchronous solution; g_{syn} is one such parameter (see equation 3.6). The results in Terman et al. (1998) provide precise conditions on combinations of parameters that ensure that the synchronous solution is stable when the inhibition is slow. Increasing g_{syn} , for example, may sometimes stabilize the synchronous solution; however, when other parameters satisfy a different relationship, increasing g_{syn} may destabilize the synchronous solution.

The size of the domain of attraction of the synchronous solution is, to a large extent, determined by the delay in the onset of inhibition. The two cells are able to fire together if the trailing cell lies within the window of opportunity determined by this delay. If the trailing cell lies outside this window, then the network typically exhibits antiphase behavior in which the cells take turns firing, although other network behavior is possible. The system may crash, for example, since the completely quiescent state is asymptotically stable.

In our analysis, we assumed that the cells and coupling are homogeneous. The effect of heterogeneities on mutually coupled basic cells with slow synapses was studied in several papers (Golomb & Rinzel, 1993; White, Chow, Ritt, Soto, & Kopell, 1998; Chow, 1998). These found that the synchronous solution is not very robust to mild levels of heterogeneities; a 5% variation in parameters was sufficient to destroy synchronous behavior. We have done a number of numerical simulations in order to study the effects of heterogeneities on the network considered in this section. Our numerical results are consistent with those in previous studies.

4 Globally Inhibitory Networks

We now consider the network described in section 2.3. Recall that in this network, E -cells excite J -cells, which in turn inhibit E -cells. The thalamic networks involved in sleep rhythms, discussed in section 5, are examples of such a network, with compound cells, to which the results of this section apply. We assume for now that there are just two E -cells, denoted by E_1 and E_2 , and there is one J -cell, which we denote as J . Larger networks are considered later. Initially, each cell is assumed to be a basic cell; generalization

for compound cells is discussed in section 4.4. The E -cells are identical to each other, but they may be different from the J . Each cell is also assumed to be excitable for fixed levels of input.

The system of equations corresponding to each E_i is

$$\begin{aligned} v_i' &= f(v_i, w_i) - g_{inh} s_j (v_i - v_{inh}) \\ w_i' &= \epsilon g(v_i, w_i) \\ s_i' &= \alpha(1 - s_i)H(v_i - \theta) - \beta s_i, \end{aligned} \quad (4.1)$$

while the equation for J is

$$\begin{aligned} v_J' &= f_J(v_J, w_J) - \frac{1}{2}(s_1 + s_2)g_{exc}(v_J - v_{exc}) \\ w_J' &= \epsilon g_J(v_J, w_J) \\ s_J' &= \alpha_J(1 - s_J)H(v_J - \theta_J) - \epsilon K_J s_J. \end{aligned} \quad (4.2)$$

Here, each synapse is direct. Indirect synapses will be needed when we discuss the stability of solutions. Note that the inhibitory variable s_j turns off on the slow timescale. The reason that we write the equations this way will become clear in the analysis. We assume that $\beta = O(1)$; however, there is no problem in extending the analysis if $\beta = O(\epsilon)$. If $v_i > \theta$, then $s_i \rightarrow \sigma_A \equiv \frac{\alpha}{\alpha + \beta}$ on the fast timescale.

Two types of network behavior are shown in Figures 8 and 9. A synchronous solution, in which each cell fires during every cycle, is shown in Figure 9. In Figure 8, each excitatory cell fires every second cycle, while J fires during every cycle. This type of solution is referred to as a clustered solution. In the following sections, we construct singular orbits corresponding to each of these solutions and then analyze their stability. The constructions then lead to conditions for when the different solutions exist and are stable.

4.1 Existence of the Synchronous Solution. We now construct a singular trajectory corresponding to a synchronous solution in phase space. As before, the trajectory for each cell lies on the left or right branch of a cubic nullcline during the silent and active phases. Which cubic a cell inhabits depends on the total synaptic input that the cell receives. Nullclines for the E_i are shown in Figure 5A and those for J in Figure 5B. Note in Figure 5A that the $s_j = 1$ nullcline lies above the $s_j = 0$ nullcline, while in Figure 5B, the $s_{tot} \equiv \frac{1}{2}(s_1 + s_2) = \sigma_A$ nullcline lies below the $s_{tot} = 0$ nullcline. This is because the E_i receive inhibition from J while J receives excitation from the E_i . We will make several assumptions concerning the flow in the following construction. These are justified later.

We begin with each cell in the active phase just after it has jumped up. These are the points labeled P_0 and Q_0 in Figure 5. Each E_i evolves down

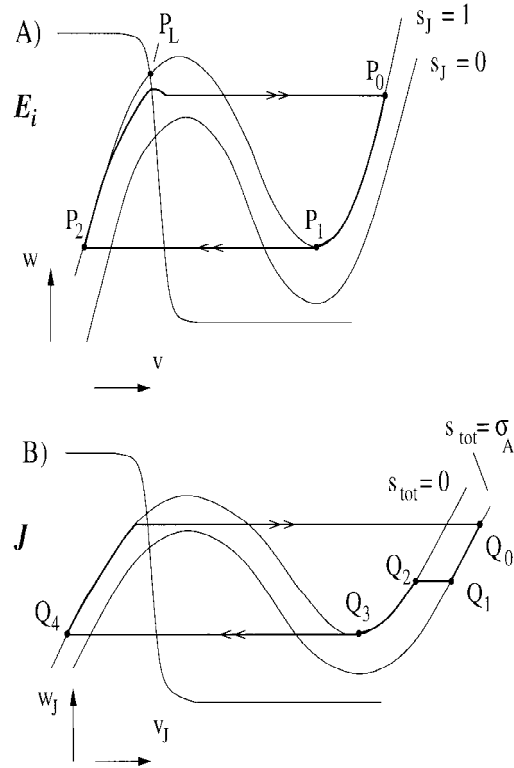


Figure 5: Nullclines for (A) E -cells and (B) J -cells in a globally inhibitory network with basic cells. The closed curves and points P_i , Q_i correspond to the singular synchronous solution discussed in the text. Note that s_j decays on the slow timescale.

the right branch of the $s_j = 1$ cubic, while J evolves down the right branch of the $s_{tot} = \sigma_A$ cubic. We assume that the E_i have a shorter active phase than J , so each E_i reaches the right knee P_1 and jumps down to the point P_2 before J jumps down. We also assume that at this time, J lies above the right knee of the $s_{tot} = 0$ cubic. J must then jump from the point Q_1 to the point Q_2 along the $s_{tot} = 0$ cubic. On the next piece of the solution, J moves down the right branch of the $s_{tot} = 0$ cubic while the E_i move up the left branch of the $s_j = 1$ cubic. When J reaches the right knee Q_3 , it jumps down to the point Q_4 along the left branch of the $s_{tot} = 0$ cubic.

Now the inhibition s_j to the E_i starts to turn off on the slow timescale. Thus, the E_i do not jump to another cubic. Instead, the trajectory for the E_i moves upward, with increasing w_i , until it crosses the w nullcline. Then each w_i starts to decrease. If this orbit is able to reach a left knee, it jumps up to

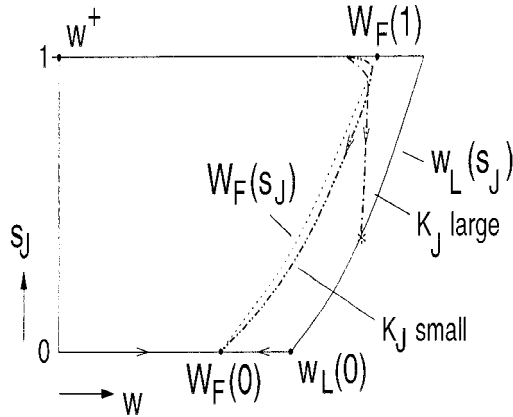


Figure 6: Slow phase plane for an E -cell. The curve $w_L(s_J)$ is the jump-up curve, which trajectories reach if K_J is large enough (--- path; cell jumps up from the point marked *). The dotted curve $W_F(s_J)$ consists of zeros of $G_L(w, s_J)$ in system 4.3; trajectories tend to the stable critical point $W_F(0)$ as $s_J \rightarrow 0$ for small K_J (- - - path). Note that $w' < 0$ for $w > W_F$.

the active phase, and this completes one cycle of the synchronous solution. When the E_i jump up, J also jumps up if it lies above the left knee of the $s_{tot} = \sigma_A$ cubic.

We now derive more quantitative conditions for when the singular synchronous solution exists. It is not at all obvious, for example, why we needed to assume that the active phase of J is longer than that for the E_i . It is also not clear what conditions are needed to ensure that the E_i are able to reach a jump-up curve and escape once they are released from inhibition. These two issues are actually closely related.

We first discuss how the E_i can reach the jump-up curve. For this, it is convenient to derive equations for the evolution of the slow variables (w_i, s_J) as was done in section 3.1. Let $\tau = \epsilon t$, denote the left branch of the cubic $f(v, w) - g_{inh}s(v - v_{inh}) = 0$ by $v = \Phi_L(w, s)$ and let $G_L(w, s) \equiv g(\Phi_L(w, s), s)$. Then each (w_i, s_J) satisfies the slow equations,

$$\begin{aligned} \dot{w} &= G_L(w, s_J) \\ \dot{s}_J &= -K_J s_J. \end{aligned} \quad (4.3)$$

The phase plane corresponding to this system is illustrated in Figure 6. There are two important curves shown in the figure. The first is the jump-up curve $w = w_L(s_J)$; this is the curve of “left knees.” The second curve, denoted by $W_F(s_J)$, corresponds to the fixed points of the first two equations

in 4.1 with the input s_j held constant. This corresponds to the w -nullcline of equation 4.3.

We need to determine when a solution $(w(\tau), s_j(\tau))$ of equation 4.3 beginning with $s_j(0) = 1$ and $w(0) < W_F(1)$ can reach the jump-up curve $w_L(s_j)$. This is clearly impossible if $W_F(1) < w_L(0)$, so we shall assume that $W_F(1) > w_L(0)$. If $w(0) > w_L(0)$ and K_j is sufficiently large, the solution will certainly reach the jump-up curve; this is because the solution will be nearly vertical, as shown in Figure 6. If, on the other hand, K_j is too small, the solution will never be able to reach the jump-up curve. This is because the solution will slowly approach the curve $W_F(s_j)$ and lie very close to this curve as s_j approaches zero. This is also shown in Figure 6. We conclude that the cells are able to escape the silent phase if the inhibitory synapses turn off sufficiently quickly and the w -values of the cells are sufficiently large when this deactivation begins. Escape is not possible for very slowly deactivating synapses (although it would be possible with slow deactivation if the cells were oscillatory for some levels of synaptic input). A biophysical interpretation of this is that escape is possible for $GABA_A$ synapses and will occur if the cell's I_T current is sufficiently deinactivated when inhibition begins to wear off.

We assume that K_j is large enough so that escape is possible. Choose W_{esc} so that the solution of equation 4.3 that begins with $s_j(0) = 1$ will be able to reach the jump-up curve only if $w(0) > W_{esc}$. The existence of the singular synchronous solution now depends on whether the E_i lie in the region where $w_i > W_{esc}$ when J jumps down to the silent phase. We claim that this requires that the active phase of J be sufficiently long. One can give a simple estimate on how long this active phase must be as follows.

Suppose that all the cells jump up when $\tau = 0$, the E_i jump down when $\tau = \tau_E$, and J jumps down when $\tau = \tau_J$. We require that $w_i(\tau_J) > W_{esc}$. Since the time the E_i spend in the silent phase before they are released from inhibition is $\tau_J - \tau_E$, this implies that $\tau_J - \tau_E$ must be sufficiently large. Hence, J 's active phase must be sufficiently longer than the E_i 's. More precisely, let w_{RK} be the value of w at the right knee of the $s_j = 1$ cubic, and let τ_L be the time it takes for the solution of the first equation in 4.1 with $s_j = 1$ to go from $w = w_{RK}$ to $w = W_{esc}$. We require that

$$\tau_J - \tau_E > \tau_L. \quad (4.4)$$

4.2 Stability of the Singular Synchronous Solution. We now demonstrate that the synchronous solution is stable if the synapse s_j is indirect and the active phase of J is sufficiently long. We start with the E_i a small distance apart, just after both have jumped up to the active phase. Assume that this causes J to fire. We will show that after one cycle, both of the E_i are so close that they must fire together again. Moreover, there is a contraction in the distance between the E -cells during each cycle.

The analysis proceeds as in the previous section. We assume that the active phases of the E_i are shorter than that of J , so that the E_i return to

the silent phase and proceed up the left branch of the $s_J = 1$ cubic before J jumps down. As the E_i move up this left branch, they approach the point P_L where the $s_J = 1$ cubic intersects the w -nullcline. (See Figure 5A.) If the active phase of J is sufficiently long, then the E_i lie as close as we please to P_L , and therefore to each other, when J jumps down. This is precisely what is required to guarantee that both will fire together during the next cycle. While in the silent phase, the E_i approach P_L at an exponential rate (in the slow timescale). This leads to a very strong compression of Euclidean distance between the cells while in the silent phase. This compression is certainly stronger than any possible expansion over the remainder of the cycle. After the J -cell falls down, s_J decays on the slow timescale. This allows the J -cell to recover so that it can fire when excited by the firing of the E -cells, and the whole cycle repeats.

We need to assume that s_J corresponds to an indirect synapse for the same reason as we did previously. When one of the E -cells fires, this causes J to fire, which sends inhibition back to the other E -cell. If s_J is direct, this causes the second E -cell to be “stepped on” on the fast timescale, and the synchronous solution cannot be stable. Note that the time between the firings of the E -cells is determined by K_J , the rate at which s_J decays. If K_J is large, the time between firings is short; it is then easier for the second cell to pass through the window of opportunity provided by the indirect synapse.

Our analysis has shown that the dynamics of the J -cell can influence the domain of attraction of the synchronous solution in several ways. If J 's active phase is long, then the E -cells lie close to each other, near P_L , when J jumps down and releases them from inhibition. Moreover, if J recovers quickly in the silent phase, then K_J can be chosen to be large. Both factors make it easier for the E -cells, once they are released from inhibition, to pass through a window of opportunity and fire during the same cycle. Hence, both enlarge the domain of attraction of the synchronous solution.

Remark 2. There are important differences between the ways in which mutually coupled and globally inhibitory networks use inhibition to synchronize oscillations. In mutually coupled networks, a second slow variable is required for the existence of the synchronized solution; it allows the cells to escape from the silent phase. The second slow variable is also required for the compression of the cells as they evolve in phase space. The existence and stability of the synchronous solution in globally inhibitory networks, on the other hand, are controlled by the dynamics of the J -cell. If the J -cell's active phase is long enough, then this pushes the E -cells, in their silent phase, to a position from which they can escape; moreover, this provides a strong compression of the E -cells. For this network, we require that the inhibition decays on the slow timescale; however, the reason is so that the J -cell can recover sufficiently. The slow recovery is not needed to allow the E -cells to escape or for compression. In fact, the domain of stability of the

synchronous solution is increased if the recovery of the J -cell and the decay of the synapses occur quickly, on the slow timescale.

4.3 Clustered Solution. We now describe the geometric construction of the singular antiphase, or clustered, solution. It suffices to consider half of a complete cycle. During this half-cycle, E_1 fires and returns to the initial position of E_2 , J fires and returns to its initial position, and E_2 evolves in the silent phase to the initial position of E_1 . By symmetry, we can then continue the solution for another half-cycle with the roles of E_1 and E_2 reversed.

When E_1 jumps up, it forces J to jump up to the right branch of the $s_{tot} = \frac{1}{2}\sigma_A$ cubic. Then E_1 moves down the right branch of the $s_j = 1$ cubic, while J moves down the right branch of the $s_{tot} = \frac{1}{2}\sigma_A$ cubic and E_2 moves up the left branch of the $s_j = 1$ cubic. We assume, as before, that E_1 's active phase is shorter than J 's active phase, so E_1 jumps down before J does so. It is possible that J lies below the right knee of the $s_{tot} = 0$ cubic at this time, in which case J also jumps down. If J lies above this right knee, then it moves down the right branch of the $s_{tot} = 0$ cubic until it reaches the right knee and then jumps down. During this time, both E_1 and E_2 move up the left branch of the $s_j = 1$ cubic.

After J jumps down, $s_j(\tau)$ slowly decreases. If E_2 is able to reach the jump-up curve, then it fires, and this completes the first half-cycle of the singular solution. Suppose that $\tau = \tau_F$ when this occurs. For this to be one-half of an antiphase solution, we need $w_2(\tau_F) = w_1(0)$, $w_1(\tau_F) = w_2(0)$, and $w_J(\tau_F) = w_J(0)$. We now derive conditions for when the antiphase solution exists. These will imply that the active phase of J cannot be too long or too short, compared with the active phase of the E_i . If J 's active phase is too long, then the network exhibits synchronous behavior as described before. If J 's active phase is too short, then the system approaches the stable quiescent state.

Suppose that E_1 and J jump up when $\tau = 0$, E_1 jumps down when $\tau = \tau_E$, and J jumps down when $\tau = \tau_J$. Let τ_L and W_{esc} be as defined in the previous section. To have a clustered solution, we require that

$$w_1(\tau_J) < W_{esc} < w_2(\tau_J). \quad (4.5)$$

The second inequality is necessary to allow E_2 to fire during the second half-cycle. The first inequality guarantees that E_1 does not fire during this half-cycle. It follows from the definitions that the first inequality is equivalent to

$$\tau_J - \tau_E < \tau_L. \quad (4.6)$$

Next we derive a similar expression for the second inequality in equation 4.5. For $w_0 < w_1$, let $\rho(w_0, w_1)$ to be the time it takes for a solution of the

first equation in 4.3 with $s_j = 1$ to go from w_0 to w_1 . The second inequality is equivalent to $\rho(w_{RK}, w_2(\tau_j)) > \tau_L$. Now,

$$\rho(w_{RK}, w_2(\tau_j)) = \rho(w_{RK}, w_2(0)) + \rho(w_2(0), w_2(\tau_j)).$$

Moreover, $w_{RK} = w_1(\tau_E)$ and $w_2(0) = w_1(\tau_F)$. Hence,

$$\rho(w_{RK}, w_2(\tau_j)) = \rho(w_1(\tau_E), w_1(\tau_F)) + \rho(w_2(0), w_2(\tau_j)).$$

Clearly, $\rho(w_2(0), w_2(\tau_j)) = \tau_j$, because E_2 lies on the $s_j = 1$ cubic for $0 < \tau < \tau_j$. It is not true that E_1 lies on the $s_j = 1$ cubic for $\tau_E < \tau < \tau_F$; however, if the first equation in 4.3 is weakly dependent on s_j , then we have that $\rho(w_1(\tau_E), w_1(\tau_F)) \approx \tau_F - \tau_E$. In this case, the second inequality in equation 4.3 is equivalent to

$$\tau_F - \tau_E + \tau_j > \tau_L. \quad (4.7)$$

One can simplify this formula if the parameter K_j is rather large. In this case, $\tau_F - \tau_j$ is small; that is, E_2 escapes the silent phase as soon as it is released from inhibition. Then equation 4.7 is approximately equivalent to

$$\tau_j > \frac{1}{2}(\tau_E + \tau_L). \quad (4.8)$$

Combining equation 4.6 and 4.8 leads to the following condition for the existence of a clustered solution if the synaptic variable s_j turns off quickly:

$$\frac{1}{2}(\tau_E + \tau_L) < \tau_j < \tau_E + \tau_L. \quad (4.9)$$

Remark 3. It is possible for both stable synchrony and stable clustering to exist for the same parameter values. Note that the domain of stability of the synchronous solution is controlled to a large extent by the size of the delay caused by the indirect inhibitory synapses. If this delay is small, the domain of stability will also be small. In this case, the synchronous solution will still be stable; however, most solutions will converge to a stable clustered solution.

4.4 Globally Inhibitory Networks with Compound Cells. The discussion in the previous subsections generalizes to globally inhibitory networks with compound cells, such as the model thalamic network in the next section. The primary difference is that each cell contains an additional slow variable, y_i , so it is necessary to consider a higher-dimensional slow phase-space. As a consequence, the jump-up curves of the previous subsections are

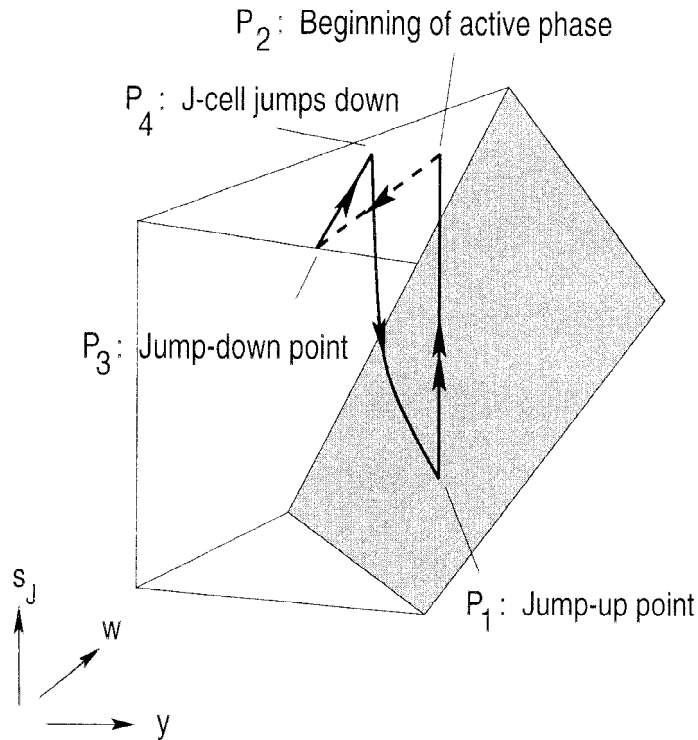


Figure 7: Three-dimensional slow phase-space for a singular synchronous periodic orbit of the globally inhibitory network. Double (single) arrows denote evolution on the fast (slow) timescale, solid (dashed) lines indicate the silent (active) phase, and points P_i are as discussed in the text. The shaded region represents the jump-up surface $w = w_L(y, s_J)$.

replaced by jump-up surfaces $\{w = w_\alpha(y, s_J)\}$, $\alpha = L$ or R , where $w_\alpha(y, s_J)$ is as in the lemma in section 3.

Figure 7 illustrates the evolution of the slow variables (w_i, y_i, s_J) for the singular synchronous solution. We begin at the point labeled P_1 on the jump-up surface $w = w_L(y, s_J)$. The E -cells then jump up, and this forces J to jump up. Hence, $s_J \rightarrow 1$. This corresponds to the segment in Figure 7 that connects P_1 to the point P_2 on the $s_J = 1$ surface. Each cell then evolves in the active phase with $s_J = 1$. As before, we assume that the active phases of the E -cells are shorter than that of J . Hence, the E -cells jump down when the (w_i, y_i) reach the jump-down curve $w_i = w_R(y_i, 1)$. This is at the point labeled P_3 in Figure 7. While J lies in the active phase, the E -cells evolve in the silent phase, but $s_J = 1$ still holds. At P_4 , J jumps down and the (w_i, y_i, s_J) evolve

until they reach the jump-up curve. This then completes one cycle of the singular solution.

The stability analysis proceeds just as in section 4.2. What is crucial for stability is that J remains active long enough. The E -cells then approach the stable fixed point on the left branch of the $s_J = 1$ surface while J is active. This provides the compression needed for stability. The construction of a clustered solution is also very similar to that described in section 4.3. We do not describe the construction here; some comments are given in the next section.

4.5 Further Remarks. The geometric constructions of the synchronous and clustered solutions extend in a straightforward manner to globally inhibitory networks with an arbitrary number of excitatory cells E_i . Of course, in a larger network there are more possibilities for clustered solutions; however, if each cluster contains (approximately) the same number of cells, then inequalities similar to equation 4.9 must be satisfied. This is similar to analysis of Terman and Wang (1995), which yields precise conditions for the existence of clustered states in a locally excitatory and globally inhibitory network model for scene segmentation. Further analysis of clustered solutions in inhibitory networks is given in Rubin and Terman (1999).

The analysis leads to simple formulas for the periods of the synchronous and clustered solutions. Let τ_J be, as above, the time cell J spends in the active phase, and let τ_S be the time for the E -cells to reach the jump-up curve after the J -cell jumps down. Then the period of the synchronous solution is simply $\tau_J + \tau_S$. Now τ_J is determined by the dynamics of the J -cell, while τ_S is primarily controlled by the rate at which the synapses turn off; this is the parameter K_J in equation 4.2. Also see Figure 11. Other parameters play a secondary role. Note, for example, that the parameter g_{syn} influences the period by controlling the slope of the jump-up curve, as shown in equation 3.6.

The synchronous and clustered solutions can exist only if trajectories are able to escape from the silent phase. Previous work on mutually inhibitory neurons has emphasized the distinction between “release” and “escape” in producing both synchronous and antiphase solutions (Wang & Rinzel, 1993). “Release” refers to the case in which the active phase of one cell ends and this releases another silent cell from inhibition. “Escape” refers to the case in which the dynamics of the inactive cell allows it to fire even if that cell receives inhibition. As pointed out in Terman et al. (1998), there is no clear distinction between escape and release when there are multiple slow processes. A silent E -cell is in some sense released when the J -cell jumps down to the silent phase. The rhythms can continue, however, only if this E -cell is able to escape the silent phase. Here we are assuming that each E -cell is excitable for constant levels of inhibition. Both escape and release are therefore needed to maintain oscillations.

5 Thalamic Network

The model for the thalamic spindle sleep rhythm falls into the framework of the network analyzed in the preceding section. The two populations of cells in the model are the thalamocortical relay (TC) cells and the thalamic reticularis (RE) cells, corresponding to the *E*-cells and *J*-cells, respectively. One difference between the spindle model and those considered earlier is that the spindle model contains numerous RE as well as TC cells. The RE cells communicate with each other through fast inhibitory synapses, as illustrated in the network shown in Figure 2.

During spindling, the network exhibits behavior similar to the clustered solution discussed in the previous section. The RE population is synchronized, while the TC cells break up into groups; cells within each group are synchronized, while cells within different groups are desynchronized. The network also exhibits completely synchronized rhythms. The synchronized rhythms arise, for example, when fast inhibition is removed from the entire network or from between the RE cells only. Recent results have also shown that the synchrony can arise if the RE population receives additional phasic excitation, corresponding to cortical input, at the delta frequency. Hence, the network can transform from clustering to synchronized behavior without any change in the inhibitory synapses.

In this section, we demonstrate how the geometric analysis helps to explain the dynamical mechanisms responsible for these rhythms and transitions between them. We begin by presenting a concrete model for the sleep rhythms and then present results of numerical simulations of this model. The numerical simulations clearly show that solutions of the model behave as predicted by the singular perturbation analysis; in particular, solutions jump up and jump down when they reach a curve (or surface) of knees. This confirms that the decomposition into fast and slow variables, as described in the previous section, provides the correct singular perturbation framework for analyzing these rhythms.

We also demonstrate how the geometric analysis leads to quantitative statements concerning the behavior of solutions. In particular, the analysis predicts correctly how the frequency of oscillations depends on parameters. The analysis also leads to precise conditions for when the network exhibits either synchronous or clustered solutions. For example, factors that enable the TC cells to synchronize are a long RE active phase, a relatively fast RE recovery, and a fast decay of inhibition. Some of these factors are inconsistent with mechanisms for synchronization in mutually coupled inhibitory networks. Finally, the analysis clarifies the roles of the various intrinsic and synaptic currents in generating a particular rhythm. We illustrate this in section 5.3, where we consider the role of the sag current, which also differs from the role of the second slow intrinsic current in mutually coupled networks.

5.1 Model. The following model contains many parameters and nonlinear functions (these are given in appendix A). The cells are modeled using the Hodgkin-Huxley formalism (Hodgkin & Huxley, 1952); the equations are very similar to those in Golomb et al. (1994).

The equations of each TC cell are:

$$\begin{aligned} v_i' &= -I_T(v_i, h_i) - I_{sag}(v_i, r_i) - I_L(v_i) - I_A - I_B \\ h_i' &= (h_\infty(v_i) - h_i)/\tau_h(v_i) \\ r_i' &= (r_\infty(v_i) - r_i)/\tau_r(v_i). \end{aligned} \quad (5.1)$$

This describes a compound cell, with h_i and r_i corresponding to w and y , respectively, and ϵ absorbed in τ_h , τ_r rather than mentioned explicitly. The terms I_T , I_{sag} , and I_L are intrinsic currents; they are given by $I_T(v, h) = g_{Ca}m_\infty^2(v)h(v - v_{Ca})$, $I_{sag}(v, r) = g_{sag}r(v - v_{sag})$, and $I_L(v) = g_L(v - v_L)$. The terms I_A and I_B represent the fast (GABA_A) and slow (GABA_B) inhibitory input from the RE cells. We model the fast inhibition I_A as in previous sections; that is, $I_A = g_A(v_i - v_A)\frac{1}{N_{TR}}\sum s_A^j$, where g_A and v_A are the maximal conductance and the reversal potential of the synaptic current. The sum is over all RE cells that send input to the i th TC cell and N_{TR} represents the maximum number of RE cells that send inhibition to a single TC cell. Each synaptic variable s_A^j satisfies the first-order equation

$$s_A^j' = \alpha_R(1 - s_A^j)H(v_R^j - \theta_R) - \beta_R s_A^j, \quad (5.2)$$

where v_R^j is the membrane potential variable of the j th RE cell. Motivated by recent experiments (Destexhe, Bal, McCormick, & Sejnowski, 1996; Destexhe & Sejnowski, 1997), we model the slow inhibition I_B somewhat differently from I_A . We first discuss, however, the model for the RE cells.

The equations of each RE cell are:

$$\begin{aligned} v_R^i' &= -I_{RT}(v_R^i, h_R^i) - I_{AHP}(v_R^i, m_i) - I_{RL}(v_R^i) - I_{RA} - I_E \\ h_R^i' &= (h_{R\infty}(v_R^i) - h_R^i)/\tau_{Rh}(v_R^i) \\ m_i' &= \mu_1[Ca]_i(1 - m_i) - \mu_2 m_i \\ [Ca]_i' &= -vI_{RT} - \gamma[Ca]_i. \end{aligned} \quad (5.3)$$

The I_{RT} , I_{AHP} , and I_{RL} represent intrinsic currents. These are given by $I_{RT}(v, h) = g_{Ca}^R m_{R\infty}^2(v)h(v - v_{Ca}^R)$, $I_{AHP}(v, m) = g_{AHP}m(v - v_K)$, and $I_{RL}(v) = g_{RL}(v - v_{RL})$. More details concerning the biophysical significance of each term are given in Golomb et al. (1994) and Terman et al. (1996).

In equation 5.3, I_{RA} represents the inhibitory input from other RE cells. It is modeled as $I_{RA} = g_{RA}(v_R^i - v_{RA})\frac{1}{N_{RR}}\sum s_{RA}^j$ where the sum is over all RE cells that send input to the i th RE cell. Each synaptic variable s_{RA}^j satisfies a

first-order equation similar to 5.2. The term I_E represents excitatory (AMPA) input from the TC cells and is expressed as $I_E = g_E(v_R^i - v_E) \frac{1}{N_{RT}} \sum s_E^j$, where the sum is over all TC cells that send excitatory input to the i th RE cell. The synaptic variables s_E^j are fast and also satisfy first-order equations similar to 5.2.

It remains to discuss how we model the slow inhibitory current I_B . Similarly to Destexhe et al. (1996), we assume that $I_B = g_B \frac{s_{bi}^4}{s_{bi}^4 + \lambda} (v_i - v_B)$ where s_{bi} , along with variable x_{bi} , satisfies

$$\begin{aligned} s'_{bi} &= k_1 H(x_{bi} - \theta_{xb})(1 - s_{bi}) - k_2 s_{bi} \\ x'_{bi} &= \frac{k_3}{N_{TR}} \left[\sum H(v_R^i - \theta_{Rb}) \right] (1 - x_{bi}) - k_4 x_{bi}. \end{aligned}$$

The parameters are such that x_{bi} can become activated (i.e., exceed θ_{xb}) only if a sufficiently large number of RE cells have their membrane potentials v_R^i above the threshold θ_{Rb} . The threshold is chosen rather large so the RE bursts must be sufficiently powerful to activate x_{bi} . Once x_{bi} becomes activated, it turns on the synaptic variable s_{bi} ; the expression s_{bi}^4 in I_B further delays the effect of the inhibition on the postsynaptic cell.

5.2 Numerical Simulations. A clustered solution is shown in Figure 8. There are three RE cells in this example, and they oscillate in synchrony at about 12.5 Hz; one of the RE cells is shown in Figure 8A. The RE cells synchronize due to excitation from the TC population. (This is discussed in more detail in section 5.3.) There are six TC cells, and they form two clusters, each oscillating at half of the RE oscillation frequency, as shown in Figure 8B. In Figure 8C, we show the time courses of the fast (s_A) and slow (s_b) inhibitory synaptic variables, respectively. Note that the fast inhibition activates during every cycle, providing the hyperpolarizing current needed to deinactivate each TC cell's I_T current. The fast inhibition is also needed to desynchronize the TC cells so they can form clusters. The slow current I_B never activates during this solution because the RE cells do not fire powerful enough bursts; that is, the membrane potentials v_R^i do not rise above the threshold $\theta_{Rb} = -25$ mV long enough to activate the variables x_{bi} .

A synchronous solution is shown in Figure 9. The parameters are exactly as in Figure 8 except we set $g_{RA} = 0$; that is, we have turned off the fast inhibition between RE cells. Note in Figure 9 that each TC cell fires during every cycle along with the RE cells. The slow inhibitory current I_B now activates during every cycle. Comparing the slow inhibitory variable with the fast inhibitory variable in Figure 9C, we see that the slow inhibition stays on longer and both turns on and turns off more gradually. Geometric analysis is useful in understanding why removing fast inhibition allows slow inhibition to activate and why this leads to synchronization of the network. This is discussed in the next subsection.

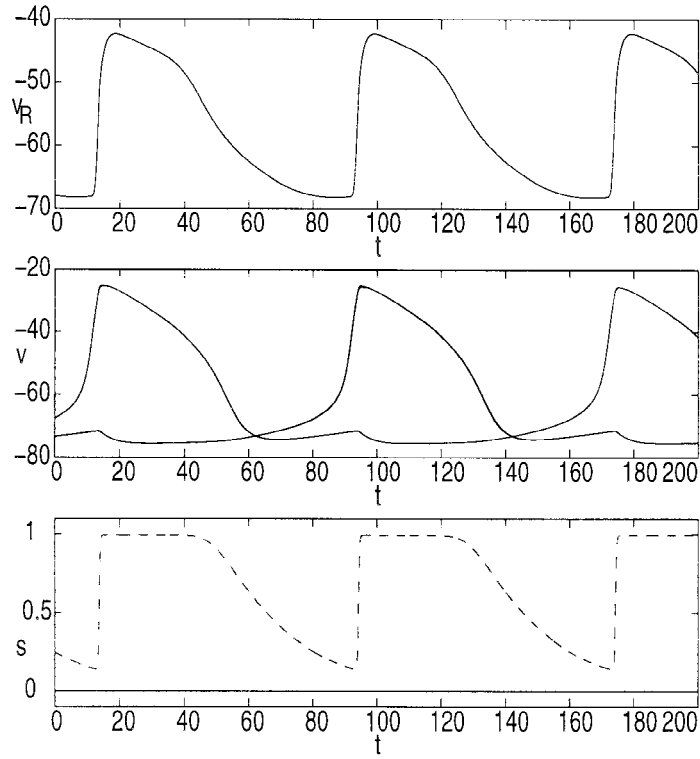


Figure 8: Numerical solution, with two TC clusters, of the thalamic network (parameter values are given in appendix A). Voltages are in mV and time is in msec. (Top) RE cell (the time course of which matches that of the RE population of three cells). (Middle) TC population of six cells, forming two clusters of three cells each. (Bottom) Inhibitory synaptic variables s_A (dashed) and s_b (solid). Note that $s_b \equiv 0$, since the RE cell bursts are not powerful enough to activate slow inhibition in this case.

In Figure 10 we plot the trajectory $(h_i(\tau), r_i(\tau), s_b(\tau))$ corresponding to the synchronous solution shown in Figure 9. We also plot the numerically computed surface of knees corresponding to the jump-up points; there is a similar jump-down surface, but it is not shown. The behavior of the trajectory is consistent with that discussed in the previous section. For example, the cells jump up when the trajectory crosses the jump-up surface of knees (approximately, since $\epsilon \neq 0$ numerically) (see Rubin & Terman, 1998, for a similar plot for the clustered solution).

Figure 11 shows a plot of the period of synchronous TC oscillations as the rate of decay of inhibition, the rate of change of h , and the parameter g_B are

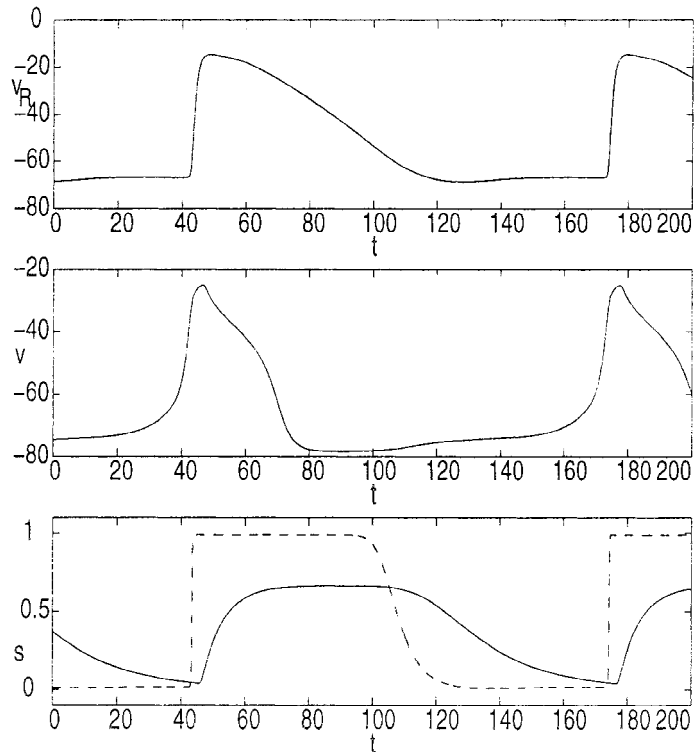


Figure 9: Numerical synchronous solution of the thalamic network (parameter values are given in appendix A). Voltages are in mV and time is in msec. (Top) RE cell (the time course of which matches that of the RE population of three cells). (Middle) TC population of six cells (synchronized). (Bottom) Inhibitory synaptic variables s_A (dashed) and s_b (solid). Note that s_A turns on and off faster than s_b , which in turn stays on longer.

separately varied. These relations can be derived from our analysis, as can predictions about the dependence of the period on other model parameters. As noted earlier, the period is given by the duration of the RE active phase (τ_I) plus the time it takes for inhibition to decay sufficiently that the TC cells can jump up (τ_S); hence, the period drops relatively sharply as the inhibitory decay rate increases. The same strong dependence, which our analysis explains, was found in the modeling work of Destexhe (1998). As the rate of change of h increases, there is essentially no change in the length of the TC silent phase (not shown) or in the period. This reflects the fact that over the parameter range considered, the TC cells are compressed close to their silent phase rest state while the RE cells are active, and then the TC cells

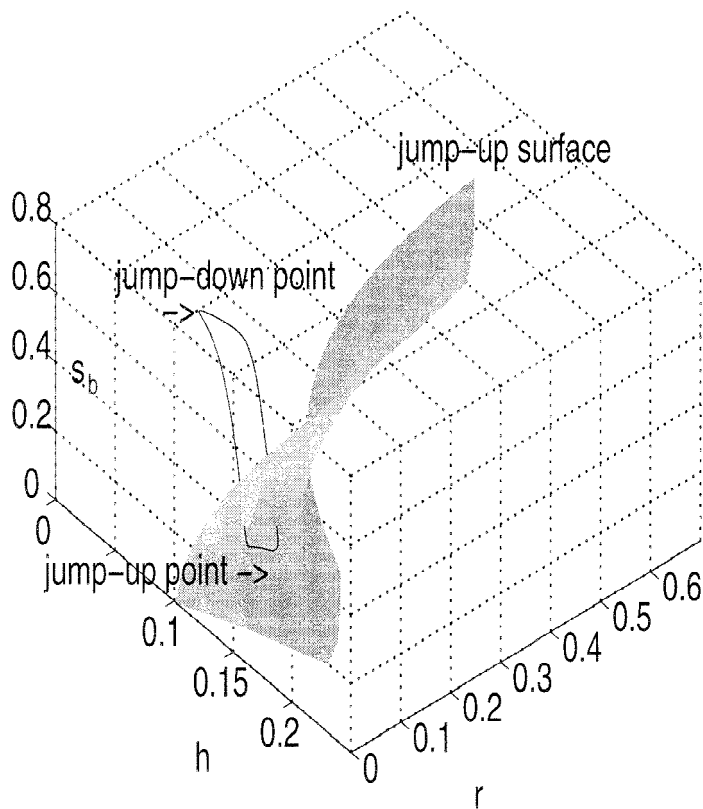


Figure 10: Numerical trajectory of a TC cell, together with jump-up surface of knees (shaded), in the (h, r, s_b) slow phase-space. The TC cell shown belongs to the synchronized population of six TC cells shown in Figure 9. Note that s_b does not immediately increase when the cell jumps up, since we have taken slow inhibitory synapses to be indirect.

evolve with little change in h after the RE cells jump down. Interestingly, g_B has little effect on period because it has little influence on τ_J, τ_S . The mild effect that does occur is due to the subtle influence of g_B on the slope of the curve of knees for the TC silent phase. This actually causes the period to increase as g_B , and hence the strength of slow inhibitory coupling, increases (see also Golomb et al., 1994).

Our numerical studies show that the synchronous and clustered solutions are robust to moderate levels of heterogeneities and variations in the parameters. This is due to the strong TC compression provided by the RE cells. For example, these solutions were not affected by heterogeneities of about 20% in gap conductances and about 5% in the TC I_T conductance.

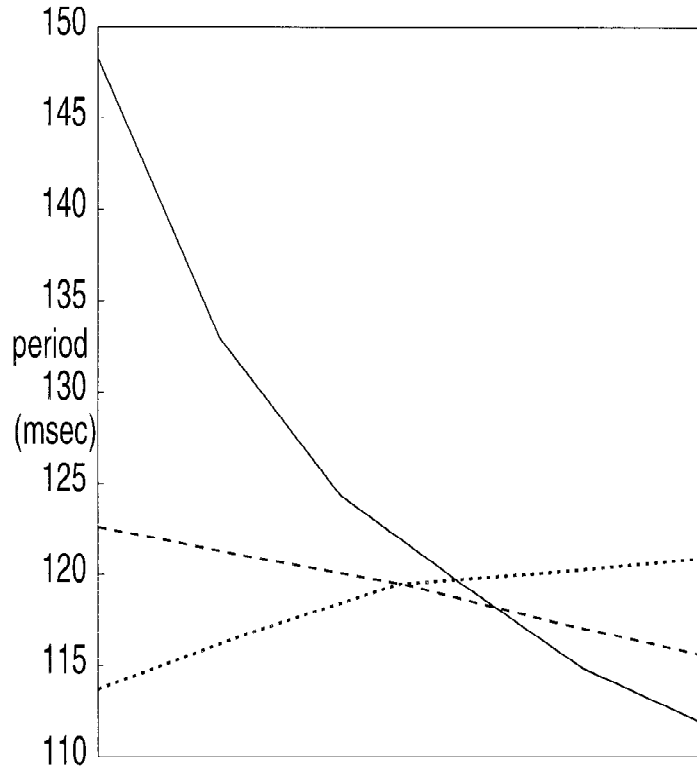


Figure 11: Period of synchronous TC oscillations versus rate of decay of inhibition ($k_2 = \beta_R$, solid curve), rate of change of h (dashed line), and g_B (dotted line) for the population shown in Figure 9. The parameters k_2, β_R were varied from 0.04 to 0.14 and were held at 0.1 for the other two curves. A parameter ϕ was factored out from τ_{h0}, τ_{h1} in the h -equation and was varied from 1.5 to 2.5; ϕ was held at 2.0 for the other curves. The parameter g_B was varied from 0.03 to 0.07 and was held at 0.05 for the other two curves. Other parameter values as given in appendix A.

Stronger TC heterogeneities tend to promote TC clustering in this model. In the resultant patterns, TC cells with similar properties fire together, independent of the way they are initially perturbed from synchrony.

5.3 Further Implications of the Analysis.

5.3.1 Removing Fast Inhibition. Fast inhibition occurs in two places: the RE cells inhibit themselves as well as the TC cells. Removing fast inhibition has different consequences for each of these synaptic connections, and

both of these help to synchronize the TC cells (see also Golomb et al., 1994; Destexhe & Sejnowski, 1997). Removing the RE-TC fast inhibition is clearly helpful for synchronization among the TC cells. This holds because the fast inhibition has a very short rise time, which follows since the fast inhibitory synapses are direct in equations 5.1 and 5.2. This short rise time corresponds to a small domain of attraction of the synchronous solution. In fact, it is precisely this inhibition that is responsible for desynchronizing the TC cells during the clustered solution.

Removing the RE-RE fast inhibition appears to be even more crucial for synchronizing the TC cells (see also Steriade, McCormick, & Sejnowski, 1993; Huguenard & Prince, 1994; Destexhe, Bal, McCormick, & Steriade, 1996; Destexhe, 1998). This allows the RE cells to fire longer, more powerful bursts, which activate the slow inhibitory current I_B . The analysis in section 4 demonstrates that long, powerful bursting of the RE cells is needed for the TC cells to synchronize, unless the desynchronizing effect of inhibition is somehow removed as discussed in Terman et al. (1996). Our numerical simulations (e.g., Figures 9–12) show, in fact, that the TC cells will synchronize even if fast inhibition is removed from within the RE population but not from the RE-TC connections.

Why removal of inhibition leads to stronger RE bursts can be easily understood by our analysis of trajectories in phase-space. This removal forces the RE cells to lie on the right branch of a different cubic while in the active phase. The cubic of the disinhibited cells lies below the cubic of the cells with inhibition. The disinhibited cells therefore jump up to larger values of membrane potential; moreover, their jump-down point (right knee) lies below the jump-down point of the inhibited cells. The disinhibited RE cells therefore have a longer active phase.

Note that the slow inhibitory current I_B , activated when RE-RE fast inhibition is removed, has slower rise and decay times than I_A . The slow rise time enhances the domain of attraction of the synchronous solution by expanding the window of opportunity. The slow decay time can help to bring the cells closer together while in the silent phase, as discussed in section 3.3 and appendix B. Hence, both effects improve the ability of the TC cells to synchronize in the absence of fast inhibition.

5.3.2 Role of the Sag Current. We view the TC cells as examples of compound cells. If one removes the sag current I_{sag} or keeps it constant, then they become basic cells. Hence, questions concerning the differences between networks with basic or compound cells are closely related to issues pertaining to the role of the sag current. The analysis in section 3 shows that in mutually coupled networks, whether the cells are basic or compound is significant. Added complexity allows the cells to escape from the silent phase and also leads to possible compression mechanisms. In globally inhibitory networks, the dynamical mechanisms responsible for the synchronous and clustered solutions are basically the same for basic or compound cells. We

therefore do not view the sag current as playing a direct role in the generation of these rhythms. Recall that oscillations arise when the cells are capable of escaping from the silent phase. The sag current helps modulate the intrinsic properties of the TC cells, and this can determine whether escape is even possible. From a more biophysical viewpoint, the sag current depolarizes the TC cells while they are silent. Hence, a stronger sag current raises the TC's resting potential. If this resting potential is too large, then inhibitory input from the RE cells may not be capable of hyperpolarizing the TC cells sufficiently to deactivate the I_T current. If this is the case, then the TC cells will not be able to fire (i.e., escape the silent phase). We note that this relates closely to some theories about mechanisms responsible for waxing and waning behavior during the spindle rhythm (Destexhe, Babloyantz, & Sejnowski, 1993; Bal & McCormick, 1996).

Within the range where escape is possible, increasing the sag current tends to enhance the TC synchronization. This occurs because the increased sag current tends to depolarize the TC cells more rapidly, leading to stronger compression.

Note that while the sag current is depolarizing during the silent phase, it is hyperpolarizing in the active phase. Hence, increasing the sag conductance lowers the left branch of the cubic corresponding to the TC cells but raises the right branch of the cubic. This decreases the voltage level to which TC cells jump up and hence the overall amplitude of TC oscillations (see Figure 12); at jump-down, the sag current is essentially deactivated, so the size of g_{sag} has little effect there. Increasing g_{sag} also tends to decrease the level of deactivation of I_T at firing, as we can show using arguments similar to the proof of the lemma in section 3, and to decrease the period of the TC cells (see Figure 12). To analyze this dependence of the period more carefully, note that the evolution of the inactivation variable h for I_T is almost linear for most of the silent phase; we can model this by $h' = \phi(1 - h)$, independent of the inhibition level. From this equation, we can approximate the time τ_k it takes for the cell to reach the curve of knees. This depends on g_{sag} , since the location of the curve of knees does. We find that $\tau_k \approx -\frac{1}{\phi} \ln(1 + h_f - h_k)$, where h_f is the h -value when the cell falls down and h_k is the h -value when it hits the curve of knees to jump up. Incorporating the dependence of h_f and h_k on g_{sag} implies that $\partial \tau_k / \partial g_{sag} < 0$; in fact, since $h_f - h_k$ is small relative to 1 and h_f, h_k depend close to linearly on g_{sag} , the dependence of τ_k on g_{sag} is almost linear as well. An analogous argument shows that the time spent in the active phase also has a roughly linear relation to g_{sag} . These nearly linear dependencies sum to yield a nearly linear relationship between overall oscillation frequency and g_{sag} , as appears in Figure 12.

5.3.3 Synchronization Among the RE Cells. The RE cells are synchronized during the spindle rhythm, primarily due to the excitation they receive from

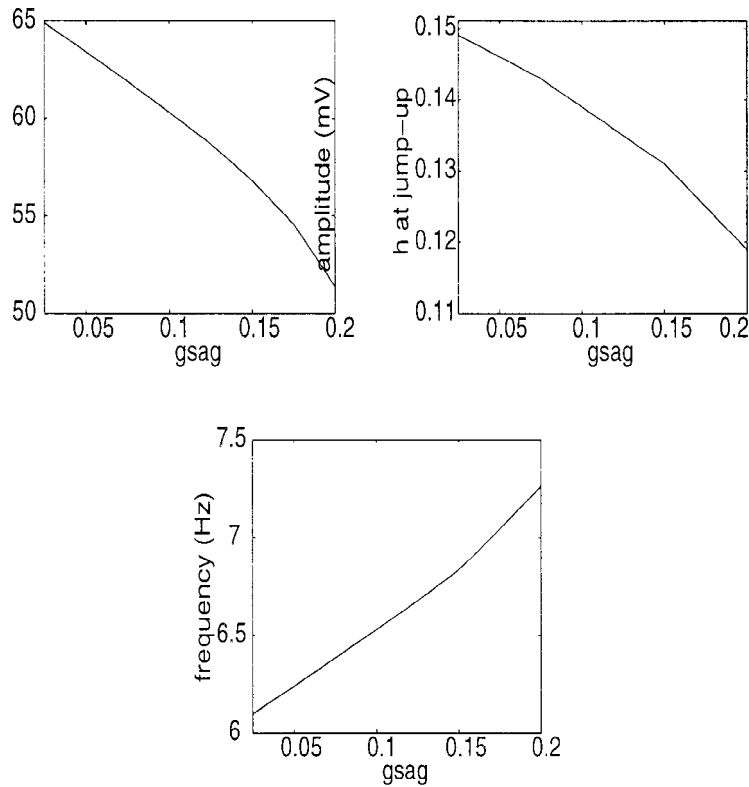


Figure 12: The effect of g_{sag} on synchronous TC oscillations. Six TC cells and three RE cells were simulated with parameter values given in appendix A.

the TC cells. Although only about half of the TC cells fire during each cycle, if each TC cell sends excitation to several RE cells, then every RE cell will receive a sufficient amount of excitation to fire during every cycle.

Experiments have also shown that the RE cells can sustain synchronized rhythms when these cells are completely isolated (Steriade, Domich, Oakson, & Deschênes, 1987; Steriade, Jones, & Llinás, 1990). In fact, these are the experiments that motivated many of the theoretical studies concerning how synchronization can arise in a population of inhibitory cells. If one considers the RE cells to be modeled as basic cells, then the conclusion of these studies is that synchronization is possible only if the decay of inhibition is sufficiently slow. However, modeling the RE cells as in equation 5.3, we consider them to be compound cells; the slow variables are h_R^i and m_i . We then conclude from our analysis of mutually coupled inhibitory cells in section 3 that synchronization is possible even if the inhibition decays quickly.

5.3.4 Cortical Inputs. Our results clearly demonstrate that globally inhibitory networks provide a natural framework for analyzing RE-TC interactions in the generation of thalamic sleep rhythms. These results are also consistent with recent work about the impact of cortical inputs in the development and manifestation of the sleep rhythms (Steriade, Curró Dossi, & Nuñez, 1991; Steriade, Nuñez, & Amzica, 1993; Steriade, 1994; Contreras, Destexhe, Sejnowski, & Steriade, 1996; Timofeev & Steriade, 1996; Contreras, Destexhe, & Steriade, 1997; Destexhe, Contreras, & Steriade, 1998). Here we review some of this work and briefly describe how it relates to our analysis.

Recent work has emphasized the importance of the cortex in the transformation of spindle oscillations into spike-and-wave-like (SW) epileptiform oscillations in the thalamus (Steriade, 1994; Steriade, Contreras, & Amzica, 1994; Contreras, Destexhe, & Steriade, 1996; Destexhe, Contreras, Sejnowski, & Steriade, 1996; Destexhe & Sejnowski, 1997; Steriade, Contreras, & Amzica, 1997; Destexhe, 1998). The experiments and modeling described in these works have suggested that this can arise without the removal of fast inhibition from the thalamus. Recall that in the mechanism we have discussed, disinhibition of the RE cells leads to more powerful RE bursts, and this permits the TC cells to synchronize. Our analysis supports the finding (Contreras, Destexhe & Steriade, 1996; Destexhe et al., 1996; Steriade et al., 1997; Destexhe, 1998) that if one does not remove the fast inhibition among the RE cells but instead induces sufficiently strong excitation from the cortex, then this will have the same effect: the RE cells will fire more powerful bursts because of the additional excitation (their cubics are lowered). Hence, $GABA_B$ inhibition of the TC cells ensues and the TC cells can synchronize, even though they receive fast inhibition from the RE cells. In particular, this explains the mechanism behind the results of Destexhe (1998), in which sufficiently strong corticothalamic excitation (achieved by blocking only cortical $GABA_A$) is found to be crucial for triggering powerful RE bursts. These bursts in turn lead to the activation of $GABA_B$ in the thalamus and the generation of synchronized ~ 3 Hz oscillations in TC and RE cells. It is interesting to note that SW discharges of pyramidal cells and interneurons in the cortex, as modeled by Destexhe, apparently result from a related interaction: excitation from TC cells induces the "spike" of prolonged firing of pyramidal cells and interneurons in the cortex, and resulting $GABA_B$ inhibition from the interneurons to the pyramidal cells enhances synchronization and maintains the subsequent "wave" of inactivity until the TC rebound and restart the cycle.

Our analysis has shown that it is possible for the TC cells to synchronize even in the presence of fast inhibition if the RE cell bursts are powerful enough. This does not, however, contradict the argument in Terman et al. (1996) that the effect of fast inhibition to the TC cells must be removed during delta. Since the RE cells fire at the slow rhythm in delta, their bursts

are completely absent (after the first cycle) while the TC cells fire. Hence, the RE cells do not produce the powerful bursts that would be needed to synchronize the TC cells if the effect of the fast inhibition remained.

5.3.5 Variations in Synchronous Oscillations. The thalamic network may exhibit other types of solutions than those discussed. This is because assumptions required for the geometric constructions of the solutions may not be satisfied for some ranges of parameter values. Subtle variations in network behavior can arise as parameters that change the underlying geometry of phase space are varied.

One possibility that arises, for certain biophysically relevant parameter values, is that the right knees of each RE cell's family of cubics lie very close to the left knees of the RE cell's cubics. In this case, each RE cell recovers almost instantly on jump-down (after a long, gradual decrease in v_R during the active phase). If the TC cells approach sufficiently close to the stable equilibrium in the silent phase while the RE cells are still active, then they can all fire as soon as they are disinhibited by RE jump-down. Hence, stable synchrony can occur here without activation of slow inhibition, even if fast inhibition decays on the fast timescale, since slow decay of inhibition was needed only to allow the RE cells to recover; this holds even though RE-TC fast inhibitory synapses are direct. (For more details, see Rubin & Terman, 1998.)

6 Discussion

Numerous articles have considered models for thalamic oscillations and mechanisms for synchronization. The RE-TC model studied here is closely related to that in Golomb et al. (1994); however, those results are based primarily on numerical studies. Here we develop, for the first time, a systematic approach for analytically studying models as complex as the thalamic networks. Related articles that deal with the role of inhibition in synchronizing bursting-like oscillations are Wang and Rinzel (1993) and Terman et al. (1998). Their conclusion is that a slow decay of inhibition is needed to obtain synchrony. This does not account, however, for synchronization of the RE-TC network in the presence of $GABA_A$ inhibition. By extending the analysis in Terman et al. (1998) to more complex networks, we are able to understand the mechanisms responsible for this. Several other articles, including van Vreeswijk et al. (1994) and Gerstner et al. (1996), have also shown that inhibition can lead to synchrony. These articles considered integrate-and-fire type models and therefore do not directly apply to the thalamic networks. One of their conclusions is that the synchronous solution must be unstable if the synapses have instantaneous onset. This is consistent with our result (also in Terman et al., 1998) that indirect synapses are needed for synchrony. Our analysis shows, however, that parameters not in the integrate-and-fire models, such as the time on the excited branch or the geometry of the curves of knees, can strongly influence when synchrony arises.

Our results clarify the multiple roles that inhibition can play in producing different rhythms. Inhibition may help to synchronize or desynchronize oscillations, depending on several factors. Fast onset of inhibition tends to desynchronize the cells, because when one cell fires, it then quickly “steps on” other cells. For this reason, we generally need to assume that the synapses are indirect for stable synchronization to occur. Slow offset of inhibition may help to synchronize the oscillations; it can lead to compression of the cells while they evolve in the silent phase. Compression (or expansion) can also take place as the cells jump up or down between the silent and active phases. This depends on the geometry of curves (or surfaces) of knees, which in turn depends on both the intrinsic and the synaptic parameters, such as g_{syn} and g_{sag} . A more powerful source of compression arises in the globally inhibitory networks. While the inhibitory cell J is active, it produces sustained inhibition to the E -cells. This forces the E -cells close to a stable fixed point and therefore close to each other. In these networks, fast offset of inhibition also helps to synchronize the cells; it helps to get cells through the narrow window of opportunity for firing.

We have demonstrated that mutually coupled networks of excitable cells with indirect fast inhibitory coupling can produce synchronized rhythms. This is not possible if the network contains only basic cells. The geometric approach helps explain why additional cellular complexity allows for synchronized rhythms. The additional complexity translates, within the framework of the geometric approach, to higher-dimensional slow manifolds. This allows the cells to escape from the silent phase. It also leads to additional sources of compression. We conclude that synchronization is possible in mutually coupled inhibitory networks if there are at least two slow variables in the intrinsic or synaptic dynamics. This has relevance for isolated RE cell populations, which can synchronize even though they include fast inhibition (Steriade et al., 1990).

Globally inhibitory networks can produce different rhythms depending on the intrinsic dynamics of the J -cells, which controls the amount of inhibition sent back to the E -cells. A rapid rate of synchronization, and a large domain of attraction for the synchronous solution, are achieved when the following factors are present: indirect synapses to provide a window of opportunity, a long J -cell active phase to enhance compression among E -cells, and a fast J -cell recovery coupled with relatively fast synaptic decay. Less powerful inhibition, or a smaller window of opportunity relative to synaptic decay rate, results in clustering among the E -cells. The network crashes if the amount of inhibition is too small. In the models for sleep rhythms, there are several possible ways to control the RE cells' bursts and therefore the emergent network behavior. More powerful RE bursts result from removal of fast inhibition from among the RE cells (Steriade, McCormick, & Sejnowski, 1993; Huguenard & Prince, 1994; Destexhe, Bal, McCormick, & Sejnowski, 1996; Destexhe, 1998) or from the addition of excitatory input from the cortex (Contreras, Destexhe, & Steriade, 1996; Destexhe, Contreras, Sejnowski,

& Steriade, 1996; Steriade et al., 1997; Destexhe, 1998). Other intrinsic RE parameters, such as a leak conductance, may also greatly influence the RE cells' dynamics. We have seen how such considerations help explain the transition between spindling, delta, and paroxysmal discharges in RE-TC networks.

The geometric analysis can lead to precise statements for when a particular rhythm is possible. For example, a TC cell can fire only if it is sufficiently hyperpolarized; this deinactivates the I_T current. A geometric interpretation is that a TC cell can fire only if, during the silent phase, it lies in the region where trajectories are able to reach the jump-up curve of knees. By considering the slow equations corresponding to the TC cells (the compound analogue of equation 4.1), one can then derive conditions for when a TC will fire. In this sense, the geometric analysis helps clarify how different parameters influence the rhythms. For example, we have seen how the analysis demonstrates that the sag current plays different roles in generating synchronized rhythms in mutually coupled and globally inhibitory networks.

We note that the geometric approach used here (see also Terman & Wang, 1995; Terman & Lee, 1997; Terman et al., 1998) is somewhat different from that used in many dynamical systems studies. All of the networks considered here consist of many differential equations, especially for larger networks. Traditionally, one would interpret the solution of this system as a single trajectory evolving in a very large-dimensional phase-space. Instead, we consider several trajectories, one corresponding to each cell, moving around in a much lower-dimensional phase-space. After reducing the full system to a system for just the slow variables, the dimension of the lower-dimensional phase-space equals the number of slow intrinsic variables and slow synaptic variables corresponding to each cell. In the worst case considered here, there are two slow variables for each compound cell and one slow synaptic variable; hence, we never have to consider phase-spaces with dimension more than three. Of course, the particular phase-space we need to consider may change, depending on whether the cells are active or silent and also depending on the synaptic input that a cell receives.

We assumed throughout that the networks were completely homogeneous. The analysis certainly extends to network models with mild heterogeneities. In this case, cells within each cluster will no longer be perfectly synchronized. They may lie on different branches of different cubic surfaces. If the cubics are sufficiently close to each other, however, the jumps will be very close to each other and almost synchrony will result.

Appendix A

The equations for the TC and RE cells in the thalamic network are given in section 5.1. As our biophysical mutually coupled network of compound cells, we considered a pair of TC cells, each governed by equation 5.1; note that in the case of basic cells without slow inhibition, these could be thought

of as simplified RE cells or TC cells. The synaptic variables in this model satisfy equation 2.6. For numerical simulations, we approximated Heaviside functions by functions of the form

$$H_\infty(v) = \frac{1}{1 + \exp(-\kappa(v - \theta))}.$$

The functions $h_\infty(v)$, $m_\infty(v)$, $r_\infty(v)$, $h_{R\infty}(v)$, and $m_{R\infty}(v)$ are assumed to be of the same form: if $\xi = h, m, r, h_R$ or m_R , then $\xi_\infty(v) = \frac{1}{1 + \exp((v + \theta_\xi)/\sigma_\xi)}$. Further, we take

$$\tau_h(v) = \tau_{h0} + \frac{\tau_{h1}}{1 + \exp((v + v_{\tau h})/\sigma_{\tau h})}$$

with $\tau_{Rh}(v)$ having an analogous form, and

$$\tau_r(v) = \tau_{r0} + \frac{\tau_{r1}}{\exp((v + v_{\tau r0})/\sigma_{\tau r0}) + \exp(-(v + v_{\tau r1})/\sigma_{\tau r1})}.$$

To generate our numerical figures, we started cells under a slight perturbation from a synchronous state. For Figures 3B and 4C, we used the following parameter values, based on Golomb et al. (1994) and Terman et al. (1996). I_T : $g_{Ca} = 2.5$, $\theta_m = 57.0$, $\sigma_m = -6.0$, $v_{Ca} = 140.0$, $\theta_h = 81.0$, $\sigma_h = 4.0$, $\tau_{h0} = 10.0$, $\tau_{h1} = 73.3$, $v_{\tau h} = 78.0$, $\sigma_{\tau h} = 3.0$; I_{sag} : $g_{sag} = 0.2$, $v_{sag} = -50.0$, $\theta_r = 75.0$, $\sigma_r = 5.5$, $\tau_{r0} = 20.0$, $\tau_{r1} = 1000.0$, $v_{\tau r0} = 71.5$, $\sigma_{\tau r0} = 14.2$, $v_{\tau r1} = 89.0$, $\sigma_{\tau r1} = 11.6$; I_L : $g_L = 0.025$, $v_L = -75.0$; I_A : $g_A = 0.4$, $v_A = -79.0$, $\alpha = 16.0$, $\beta = 4.0$, $\theta_x = 0.1$, $\kappa = 100.0$, $\epsilon\alpha_x = 0.3$, $\epsilon\beta_x = 0.1$, $\theta_{syn} = -50.0$. We did not include slow inhibition here.

To generate the clustered solution displayed in Figure 8, we used the following parameter values, also based on Golomb et al. (1994) and Terman et al. (1996). Six TC cells: I_T : $g_{Ca} = 1.5$, $\theta_m = 59.0$, $\sigma_m = -9.0$, $v_{Ca} = 90.0$, $\theta_h = 82.0$, $\sigma_h = 5.0$, $\tau_{h0} = 66.6$, $\tau_{h1} = 333.3$, $v_{\tau h} = 78.0$, $\sigma_{\tau h} = 1.5$; I_{sag} : $g_{sag} = 0.15$, $v_{sag} = -40.0$, $\theta_r = 75.0$, $\sigma_r = 5.5$, $\tau_{r0} = 20.0$, $\tau_{r1} = 1000.0$, $v_{\tau r0} = 71.5$, $\sigma_{\tau r0} = 14.2$, $v_{\tau r1} = 89.0$, $\sigma_{\tau r1} = 11.6$; I_L : $g_L = 0.2$, $v_L = -76.0$; I_A : $g_A = 0.1$, $v_A = -84.0$, $\alpha_R = 8.0$, $\beta_R = 0.05$, $\theta_R = -50.0$, $\kappa_A = 2.0$; I_B : $g_B = 0.05$, $v_B = 95.0$, $\lambda = 10^{-4}$, $k_1 = 0.1$, $k_2 = 0.05$, $\theta_{xb} = 0.8$, $\kappa_{xb} = 0.02$, $k_3 = 0.5$, $k_4 = 0.005$, $\theta_{Rb} = -25.0$, $\kappa_b = 2.0$. Three RE cells: I_{RT} : $g_{Ca}^R = 2.0$, $\theta_m^R = 52.0$, $\sigma_m^R = -9.0$, $v_{Ca}^R = 90.0$, $\theta_h^R = 72.0$, $\sigma_h^R = 2.0$, $\tau_{h0}^R = 66.6$, $\tau_{h1}^R = 333.3$, $v_{\tau h}^R = 78.0$, $\sigma_{\tau h}^R = 1.0$; I_{AHP} : $g_{AHP} = 0.1$, $v_K = -90.0$, $\mu_1 = 0.02$, $\mu_2 = 0.025$, $v = 0.01$, $\gamma = 0.08$; I_{RL} : $g_{RL} = 0.3$, $v_{RL} = -76.0$; I_{RA} : $g_{RA} = 0.25$, $v_{RA} = -84.0$, other parameters as in I_A for the TC cells; I_E : $g_E = 0.6$, $v_E = 0$, $\alpha_E = 2.0$, $\beta_E = 0.05$, $\theta_E = -35.0$, $\kappa_E = 2.0$. [Note that in the current I_E , the variables s_E^i satisfy an equation of the form (5.2), with the parameters α_E, \dots replacing α_R, \dots .]

To generate the synchronous solution displayed in Figures 9 and 10, we used the same parameter values except $\alpha = 16$, $\beta = 0.2$, $\sigma_{\tau h} = 3.0$, $\sigma_{\tau h}^R = 2.0$, $g_{RA} = 0$. By setting $g_{RA} = 0$, we removed the RE-RE fast inhibition; for $\alpha_R = 16$, $\beta_R = 0.2$ with the same initial conditions and $g_{RA} = 0.25$, the solution forms two clusters, but slow inhibition is slightly activated and it eventually destabilizes, while for $g_{RA} = 0.5$, the solution forms two clusters without activation of slow inhibition. Finally, for Figures 11 and 12, we used the above parameter values except certain parameters were varied as discussed in the text and figure captions and $\tau_{h0} = 100.0$, $\tau_{h1} = 500.0$, $\sigma_{\tau h} = 3.0$, $\tau_{h0}^R = 100.0$, $\tau_{h1}^R = 500.0$, $\sigma_{\tau h}^R = 2.0$.

Remark 4. We assumed in the proof of the lemma in section 3 that for compound cells, $f_y > 0$ in the silent phase, while $f_y < 0$ in the active phase. This is justified for the TC cell model for the following reason. Note that y corresponds to the variable r ; hence, $f_y = -g_{sag}(v - v_{sag})$. Since $v_{sag} \approx -40$ mV typically, while v ranges from around -80 mV in the silent phase to at least -30 mV in the active phase, the result follows.

Remark 5. We claimed in remark 1 that $|\frac{\partial w_R}{\partial y}|$ is quite small. This is also shown numerically in Figure 3B. We can understand analytically why this is so by recalling, from the proof of the lemma, that $\frac{\partial w_\alpha}{\partial y} = -\frac{f_y}{f_w}$ for $\alpha = L$ or R corresponding to the silent or active phase respectively. From equation 5.1,

$$\frac{\partial w_\alpha}{\partial y} = -\frac{g_{sag}(v - v_{sag})}{g_{Ca}m_\infty^2(v)(v - v_{Ca})}. \quad (\text{A.1})$$

Typical values are $g_{sag} \approx .04$ up to 2.0 , $v_{sag} \approx -40$ mV, $g_{Ca} \approx 2.5$, $v_{Ca} \approx 140$ mV. In the silent phase, $m_\infty(v)$ is small, so the numerator and denominator in equation A.1 have similar magnitudes, even though $v \approx -80$ mV. In the active phase, however, $m_\infty(v) \approx 1$ while $v \approx 0$, typically. Hence, $|\frac{\partial w_R}{\partial y}|$ is quite small.

Appendix B

Consider a pair of compound cells in the active phase, with mutual inhibitory coupling. Suppose that the cells are perturbed from synchrony such that the lead cell falls down to the silent phase at time τ_1 and the following cell falls down at time $\tau_2 > \tau_1$. Assume slow decay of inhibition ($\beta = \epsilon K$), although the analysis simplifies otherwise (see below). During the silent phase, for $\tau \geq \tau_2$, the slow dynamics of the two cells are given by

$$\begin{aligned} \dot{w} &= g(v, w) \\ \dot{y} &= h(v, y) \\ \dot{s} &= -Ks, \end{aligned} \quad (\text{B.1})$$

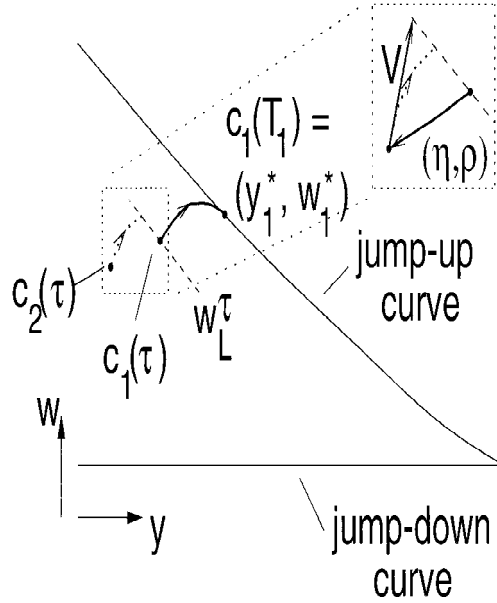


Figure 13: The set-up for analysis of compression in the silent phase in two dimensions (i.e., assuming s is fixed). The picture generalizes naturally to 3D when s is included as another slowly evolving variable. Cell 1 jumps up first, with $\tau = T_1$, at (y_1^*, w_1^*) . The larger dotted square shows a blow-up of the smaller dotted square, in which the vectors V and (η, ρ) are defined.

where v satisfies $v = \Phi_L(w, y, s)$ and $\dot{} = \frac{d}{d\tau}$. Let $V(\tau) = (g(w, v), h(y, v), -Ks)$. The equation of variations that describes the evolution of tangent vectors to the flow of equation B.1 is

$$\begin{aligned}\delta \dot{w} &= -a^w \delta w - b^w \delta y - c^w \delta s \\ \delta \dot{y} &= -a^y \delta w - b^y \delta y - c^y \delta s \\ \delta \dot{s} &= -K \delta s,\end{aligned}\tag{B.2}$$

where $a^w = -\partial g / \partial w$, $b^w = -\partial g / \partial y = -\partial g / \partial v \cdot \partial \Phi_L / \partial y$, and so on.

Fix the cell that jumps up out of the silent phase first as cell 1 and call the other cell 2. Let T_i denote the jump-up time of cell i and restrict to $\tau \in [\tau_2, T_1]$. Let $(\eta(\tau), \rho(\tau), \sigma(\tau))$ denote the vector from the position of cell 1 to that of cell 2, such that (η, ρ, σ) satisfies equation B.2; see Figure 13 for a two-dimensional representation of this set-up.

Next, let $w_L(y, s)$ denote the projection of the left surface of knees to (w, y, s) -space and let $(a, b, c) = \nabla[w_L(y_1(T_1), s(T_1)) - w(T_1)] = (-1, \frac{\partial w_L}{\partial y}(y_1(T_1), s(T_1)), \frac{\partial w_L}{\partial s}(y_1(T_1), s(T_1)))$. Let w_L^τ denote the physical translate

of $w_L(y, s)$ to the position of cell 1 at time τ ; for example, at time τ_2 , cell 1 lies in $w_L^{\tau_2}$. Again, see Figure 13.

We define the time $T(\tau)$ as the time for cell 2 to flow to its first intersection with w_L^{τ} . This satisfies

$$(a, b, c) \cdot \left[(\eta, \rho, \sigma) + \int_0^{T(\tau)} V(\tau + \xi) d\xi \right] = 0, \quad (\text{B.3})$$

where V is evaluated along the path of cell 2 (see Figure 13), but

$$\begin{aligned} \int_0^{T(\tau)} V(\tau + \xi) d\xi &= \int_0^{T(\tau)} (V(\tau) + \xi \dot{V}(\tau) + O(\xi^2)) d\xi \\ &= V(\tau)T(\tau) + O(T^2). \end{aligned} \quad (\text{B.4})$$

For small perturbations from synchrony, if the vector field of equation B.1 is $O(1)$, then the $O(T^2)$ term in equation B.4 can be neglected. Substituting the approximation equation B.4 into B.3 yields, at leading order,

$$T(\tau) = -\frac{(a, b, c) \cdot (\eta, \rho, \sigma)}{(a, b, c) \cdot V} = \frac{\eta - b\rho - c\sigma}{-g(w_2, v_2) + bh(y_2, v_2) - cKs_2}, \quad (\text{B.5})$$

since $a = -1$. Henceforth, we omit the arguments indicating evaluation along the path of cell 2 when this is clear.

A sufficient condition for compression in the silent phase is that $\dot{T}(\tau) < 0$ for $\tau \in [\tau_2, T_1]$. Thus, we proceed to compute $\dot{T}(\tau)$. Since (η, ρ, σ) and $V(\tau)$ satisfy equation B.2, we differentiate, substitute from B.2, and simplify to obtain

$$\dot{T}(\tau) = \frac{[V(\tau) \times (\eta, \rho, \sigma)] \cdot [(a, b, c) \cdot DV] \times (a, b, c)^\dagger}{((a, b, c) \cdot V(\tau)^\dagger)^2}, \quad (\text{B.6})$$

where \dagger denotes transpose.

Geometrically, the determinant of three vectors gives the volume of the parallelepiped they bound. The numerator of $\dot{T}(\tau)$ consists of such a determinant, with the three edges of the parallelepiped given by the vector field, the vector from the position of cell 1 to that of cell 2, and a third vector. This last vector relates the linearization of the vector field to the gradient of the translate of the surface of knees.

Next, consider

$$\begin{aligned} Z &\equiv (Z_1, Z_2, Z_3) := V \times (\eta, \rho, \sigma) \\ &= (\sigma h + \rho Ks, -\sigma g - \eta Ks, \rho g - \eta h) \\ &= ((h, -Ks) \wedge (\rho, \sigma), (\eta, \sigma) \wedge (g, -Ks), (g, h) \wedge (\eta, \rho)). \end{aligned} \quad (\text{B.7})$$

Differentiating equation B.7 and using B.2 gives, in system form,

$$\begin{aligned}\dot{Z}_1 &= -(b^y + K)Z_1 + a^y Z_2 \\ \dot{Z}_2 &= b^w Z_1 - (a^w + K)Z_2 \\ \dot{Z}_3 &= c^w Z_1 + c^y Z_2 - (a^w + b^y)Z_3.\end{aligned}\tag{B.8}$$

For basic cells, without the current y , equation B.6 simplifies to

$$\dot{T}(\tau) = \frac{\sigma g + \eta K s}{(g + c K s)^2} (c(a^w - K) + c^w) = \frac{-Z_2}{(g + c K s)^2} (c(a^w - K) + c^w).$$

Moreover, $Z_1 \equiv 0$, so $\dot{Z}_2 = -(a^w + K)Z_2$. Hence, the sign of $Z_2(\tau)$ is invariant for $\tau \in [\tau_2, T_1]$. In Terman et al. (1998), $Z_2(\tau_2) = (w_1(\tau_2) - w_2(\tau_2))Ks_2(\tau_2) < 0$, which implies that $-Z_2(\tau_2) > 0$. Thus, the sign of $\dot{T}(\tau)$ matches that of $(c(a^w - K) + c^w)$ (Terman et al. use λ_1 to denote c). By showing that this quantity is negative for all relevant τ for $K < a_-$ (case I in Terman et al., 1998), Terman et al. achieve a sufficient condition for compression in the silent phase.

In general, one can compute the signs of a, b, c as well as a^w, b^w, \dots (see, e.g., the lemma in section 3) and then can use equations B.6 and B.8 to derive compression conditions for the silent phase. Simplifications facilitate this process in certain cases even for compound cells. For example, $\sigma = \dot{\sigma} = 0$ during the silent phase for E cells in a globally inhibitory network as well as for much of the silent phase for mutually coupled cells with fast synaptic decay. In the latter case, however, an adjustment must be made to compensate for the fact that one cell loses inhibition before the other; we omit details and explicit computations here.

Acknowledgments

We thank N. Kopell for her very useful comments. Research for this article was supported in part by the NSF grants DMS-9423796 and DMS-9804447. Some of the research was done while the authors were visiting the IMA at the University of Minnesota.

References

- Bal, T., & McCormick, D. A. (1996). What stops synchronized thalamocortical oscillations? *Neuron*, *17*, 297–308.
- Bush, P., & Sejnowski T. (1996). Inhibition synchronizes sparsely connected cortical neurons within and between columns of realistic network models. *J. Comp. Neurosci.*, *3*, 91–110.
- Chow, C. C. (1998). Phase-locking in weakly heterogeneous neuronal networks. *Physica D*, *118*, 343–370.

- Contreras, D., Destexhe, A., Sejnowski, T. J., & Steriade, M. (1996). Control of spatiotemporal coherence of a thalamic oscillation by corticothalamic feedback. *Science*, *274*, 771–774.
- Contreras, D., Destexhe, A., & Steriade, M. (1996). Cortical and thalamic participation in the generation of seizures after blockage of inhibition. *Soc. Neurosci. Abst.*, *22*, 2099.
- Contreras, D., Destexhe, A., & Steriade, M. (1997). Spindle oscillations during cortical spreading depression in naturally sleeping cats. *Neuroscience*, *77*, 933–936.
- Destexhe, A. (1998) Spike-and-wave epileptic oscillations based on the properties of GABA_B receptors. *J. Neurosci.*, *18*, 9099–9111.
- Destexhe, A., Babloyantz, A., & Sejnowski, T. J. (1993). Ionic mechanisms for intrinsic slow oscillations in thalamic relay and reticularis neurons. *Biophys. J.*, *65*, 1538–1552.
- Destexhe, A., Bal, T., McCormick, D. A., & Sejnowski, T. J. (1996). Ionic mechanisms underlying synchronized oscillations and propagating waves in a model of ferret thalamic slices. *J. Neurophysiol.*, *76*, 2049–2070.
- Destexhe, A., Contreras, D., Sejnowski, T. J., & Steriade, M. (1996). Cortical projections to the thalamic reticular nucleus may control the spatiotemporal coherence of spindle and epileptic oscillations. *Soc. Neurosci. Abst.*, *22*, 2099.
- Destexhe, A., Contreras, D., & Steriade, M. (1998). Mechanisms underlying the synchronizing action of corticothalamic feedback through inhibition of thalamic relay cells. *J. Neurophysiol.*, *79*, 999–1016.
- Destexhe, A., McCormick, D. A., & Sejnowski, T. J. (1993). A model for 8–10 Hz spindling in interconnected thalamic relay and reticularis neurons. *Biophys. J.*, *65*, 2474–2478.
- Destexhe, A., & Sejnowski, T. J. (1997). Synchronized oscillations in thalamic networks: Insights from modeling studies. In M. Steriade, E. G. Jones, & D. A. McCormick (Eds.), *Thalamus*. Amsterdam: Elsevier.
- Gerstner, W., van Hemmen, J. L., & Cowan, J. (1996). What matters in neuronal locking? *Neural Comp.*, *8*, 1653–1676.
- Golomb, D., & Rinzel, J. (1993). Dynamics of globally coupled inhibitory neurons with heterogeneity. *Phys. Rev. E*, *48*, 4810–4814.
- Golomb, D., & Rinzel, J. (1994). Clustering in globally coupled inhibitory neurons. *Physica D*, *72*, 259–282.
- Golomb, D., Wang, X.-J., & Rinzel, J. (1994). Synchronization properties of spindle oscillations in a thalamic reticular nucleus model. *J. Neurophysiol.*, *72*, 1109–1126.
- Golomb, D., Wang, X.-J., & Rinzel, J. (1996) Propagation of spindle waves in a thalamic slice model. *J. Neurophysiol.*, *75*, 750–769.
- Hodgkin, A. L., & Huxley, A. F. (1952). A quantitative description of membrane current and its application to conduction and excitation in nerve. *J. Physiol. (London)*, *117*, 500–544.
- Huguenard, J., & Prince, D. (1994). Clonazepam suppresses GABA_B-mediated inhibition in thalamic relay neurons. *J. Neurophysiol.*, *71*, 2576–2581.

- Kim, U., Bal, T., & McCormick, D. A. (1995). Spindle waves are propagating synchronized oscillations in the ferret LGNd in vitro. *J. Neurophysiol.*, *74*, 1301–1323.
- Kopell, N., & LeMasson, G. (1994). Rhythmogenesis, amplitude modulation and multiplexing in a cortical architecture. *Proc. Nat. Acad. Sci. (USA)*, *91*, 10586–10590.
- LoFaro, T., & Kopell, N. (In press). Time regulation in a network reduced from voltage-gated equations to a one-dimensional map. *J. Math. Biology*.
- Rinzel, J. (1987). A formal classification of bursting mechanisms in excitable systems. In A. M. Gleason (Ed.), *Proceedings of the International Congress of Mathematics* (pp. 1578–1593). Providence, RI: AMS.
- Rinzel, J., Terman, D., Wang, X.-J., & Ermentrout, B. (1998). Propagating activity patterns in large-scale inhibitory neuronal networks. *Science*, *279*, 1351–1355.
- Rowat, P., & Selverston, A. (1997). Oscillatory mechanisms in pairs of neurons connected with fast inhibitory synapses. *J. Comp. Neurosci.*, *4*, 103–127.
- Rubin, J., & Terman, D. (1998). *Geometric analysis of population rhythms in synaptically coupled neuronal networks*. Unpublished manuscript, IMA Preprint Series 1596, University of Minnesota.
- Rubin, J., & Terman, D. (1999). Analysis of clustered firing patterns in synaptically coupled networks of oscillators. Manuscript submitted for publication.
- Skinner, F., Kopell, N., & Marder, E. (1994). Mechanisms for oscillation and frequency control in networks of mutually inhibitory relaxation oscillators. *J. Comp. Neurosci.*, *1*, 69–87.
- Somers, D., & Kopell, N. (1993). Rapid synchronization through fast threshold modulation. *Biol. Cyber.*, *68*, 393–407.
- Steriade, M. (1994). Coherent activities in corticothalamic networks during resting sleep and their development into paroxysmal events. In G. Buzsáki, R. Llinás, W. Singer, A. Berthoz, & Y. Chertsen (Eds.), *Temporal coding in the brain*. New York: Springer-Verlag.
- Steriade, M., Contreras, D., & Amzica, F. (1994). Synchronized sleep oscillations and their paroxysmal developments. *TINS*, *17*, 199–208.
- Steriade, M., Contreras, D., & Amzica, F. (1997). The thalamocortical dialogue during wake, sleep, and paroxysmal oscillations. In M. Steriade, E. G. Jones, & D. A. McCormick (Eds.), *Thalamus*. Amsterdam: Elsevier
- Steriade, M., Curró Dossi, R., & Nuñez, A. (1991). Network modulation of a slow intrinsic oscillation of cat thalamocortical neurons implicated in sleep delta waves: Cortically induced synchronization and brainstem cholinergic suppression. *J. Neurosci.*, *11*, 3200–3217.
- Steriade, M., Domich, L., Oakson, G., & Deschênes, M. (1987). Abolition of spindle oscillations in thalamic neurons disconnected from nucleus reticularis thalami. *J. Neurophysiol.*, *57*, 260–273.
- Steriade, M., Jones, E. G., & Llinás, R. R. (1990). *Thalamic oscillations and signaling*. New York: Wiley
- Steriade, M., McCormick, D. A., & Sejnowski, T. J. (1993). Thalamocortical oscillations in the sleeping and aroused brain. *Science*, *262*, 679–685.

- Steriade, M., Nuñez, A., & Amzica, F. (1993). Intracellular analysis of relations between the slow (< 1 Hz) neocortical oscillation and other sleep rhythms of the electroencephalogram. *J. Neurosci.*, *13*, 3266–3283.
- Terman, D., Bose, A., & Kopell, N. (1996). Functional reorganization in thalamo-cortical networks: Transition between spindling and delta sleep rhythms. *Proc. Natl. Acad. Sci. (USA)*, *93*, 15417–15422.
- Terman, D., Kopell, N., & Bose, A. (1998). Dynamics of two mutually coupled inhibitory neurons. *Physica D*, *117*, 241–275.
- Terman, D., & Lee, E. (1997). Partial synchronization in a network of neural oscillators. *SIAM J. Appl. Math.*, *57*, 252–293.
- Terman, D., & Wang, D. L. (1995). Global competition and local cooperation in a network of neural oscillators. *Physica D*, *81*, 148–176.
- Timofeev, I., & Steriade, M. (1996). Low-frequency rhythms in the thalamus of intact-cortex and decorticated cats. *J. Neurophysiol.*, *76*, 4152–4168.
- Traub, R. D., & Miles, R. (1991). *Neuronal networks of the hippocampus*. New York: Cambridge University Press
- van Vreeswijk, C., Abbott, L., & Ermentrout, G. B. (1994). When inhibition, not excitation synchronizes neural firing. *J. Comp. Neurosci.*, 313–321.
- Wang, X.-J., Golomb, D., & Rinzler, J. (1995). Emergent spindle oscillations and intermittent burst firing in a thalamic model: Specific neuronal mechanisms. *Proc. Natl. Acad. Sci. (USA)*, *92*, 5577–5581.
- Wang, X.-J., & Rinzler, J. (1992). Alternating and synchronous rhythms in reciprocally inhibitory model neurons. *Neural Comp.*, *4*, 84–97.
- Wang, X.-J., & Rinzler, J. (1993). Spindle rhythmicity in the reticularis thalamic nucleus: Synchronization among mutually inhibitory neurons. *Neuroscience*, *53*, 899–904.
- Wang, X.-J., & Rinzler, J. (1995). Oscillatory and bursting properties of neurons. In M. A. Arbib (Ed.), *The handbook of brain theory and neural networks* (pp. 686–691). Cambridge, MA: MIT Press.
- Whittington, M. A., Traub, R. D., & Jefferys, J. G. R. (1995). Synchronized oscillations in interneuron networks driven by metabotropic glutamate receptor activation. *Nature*, *373*, 612–615.
- White, J., Chow, C. C., Ritt, J., Soto, C., & Kopell, N. (1998). Synchronization and oscillatory dynamics in heterogeneous, mutually inhibited neurons. *J. Comp. Neurosci.*, *5*, 5–16.